International Journal of Mechanical Sciences 128–129 (2017) 70–93

Contents lists available at ScienceDirect

International Journal of Mechanical Sciences

journal homepage: www.elsevier.com/locate/ijmecsci

Anisotropy and plastic flow in the circular bulge test

L.C. Reis[a], P.A. Prates[a,*], M.C. Oliveira[a], A.D. Santos[b], J.V. Fernandes[a]

[a] CEMMPRE, Department of Mechanical Engineering, University of Coimbra, Pólo II, Rua Luís Reis Santos, Pinhal de Marrocos, 3030-788 Coimbra, Portugal
[b] Faculty of Engineering, University of Porto, Rua Dr. Roberto Frias, 4200-465 Porto, Portugal

ARTICLE INFO

Keywords:
Circular bulge test
Stress *vs.* strain curve
Anisotropic metal sheets
Membrane theory
Numerical simulation

ABSTRACT

The procedures for obtaining the stress *vs.* strain curve from the circular bulge test are investigated in detail resorting to finite element analysis. Particular attention is given to in-plane anisotropic materials for which remains a lack of knowledge about the distributions near the pole of the bulge specimen of variables such as the surface radius of curvature, sheet thickness, principal stresses and strains as well as stress and strain paths. This study seeks to understand and evaluate the errors inherent to the commonly used experimental procedure for assessing the hardening curve from the bulge test. The procedure assumes that the stress path at the pole is equibiaxial. An empirical equation relating the stress path with the strain path at the pole of the cap is suggested to improve the determination of the biaxial stress *vs.* strain curve, which holds particular prominence in cases of strongly anisotropic sheets.

1. Introduction

Sheet metal forming processes are demanded to manufacture components for the automotive, aeronautics and other industries. The finite element method (FEM) is commonly used nowadays for simulating and optimizing sheet metal forming processes. However, the numerical simulation results are dependent on the convenient characterization and modelling of the mechanical behaviour of metal sheets. Whatever the constitutive model used in the simulations (*i.e.* hardening law and anisotropic yield criterion), the strategies for identifying its parameters as well as the experimental tests and procedures used in the analysis play an important role in the characterization of the metal sheets mechanical behaviour [1–8]. The parameters of the models are generally determined with recourse to tensile and other experimental tests, such as shear, cruciform and bulge [9].

The circular bulge test under hydraulic pressure allows achieving relatively high strain values before necking and enables the definition of the hardening law for a wide range of plastic deformation [10]. The periphery of the metal sheet is immobilized through a drawbead, which prevents the peripheral region of the sheet from moving into the radial direction [11–13]. Then, a hydraulic pressure is applied on the inner surface of the sheet, promoting an approximately spherical shape in the region near the pole of the cap and inside a circle of constant latitude [14,15]. Under these conditions, a biaxial stress path occurs at the pole of the cap.

For evaluating the stress *vs.* strain curve, the evolutions of pressure, radius of curvature and strain at the pole of the cap should be recorded during the test. The measurements of radius of curvature and strain can be performed by a spherometer and an extensometer, respectively [16,17]. An optical system can replace these mechanical systems with advantages, since it enables the description of the geometry and strain distributions on the sheet surface during the bulge test [18,19]. In both cases, the membrane theory that relates the stresses at the pole with the pressure, radius of curvature and sheet thickness must be used [20].

The analysis of the bulge test results, including the application of the membrane theory, still presents uncertainties, despite of the recent recommended procedure by ISO 16808 (2014) [21]. In fact, the accurate evaluation of the stress *vs.* strain curves depends on assumptions and simplifications, whose assessment are still under study. For example, in a recent study Mulder et al. [22] examined the validity and the conditions for using the membrane theory, which includes issues related to the geometry of the cap that affects the evaluation of the radii of curvature near the pole and the equibiaxial stress state assumption in case of in-plane anisotropic materials. They showed that the spherical function can be successfully replaced by the ellipsoid function, for describing the bulge surface up to large distances from the pole of the cap, in order to estimate the curvature radius. This allows increasing the data to be considered without loss of accuracy, since it enables the reduction of the scatter. In case of an in-plane anisotropic material, Mulder et al. [22] concluded that the test conditions force the material towards an equibiaxial strain state and the deviations of the average stress from the equibiaxial stress are less than 3%, for an in-plane

* Corresponding author.
E-mail addresses: luis.reis@dem.uc.pt (L.C. Reis), pedro.prates@dem.uc.pt (P.A. Prates), marta.oliveira@dem.uc.pt (M.C. Oliveira), abel@fe.up.pt (A.D. Santos), valdemar.fernandes@dem.uc.pt (J.V. Fernandes).

http://dx.doi.org/10.1016/j.ijmecsci.2017.04.007
Received 22 November 2016; Received in revised form 1 March 2017; Accepted 10 April 2017
Available online 13 April 2017
0020-7403/

anisotropic material described by the Hill'48 criterion, with values of the anisotropy coefficient, r, for angles of 0, 45 and 90°, such that $r_0 = 0.5$ and $r_{45} = r_{90} = 1.0$ [23]. Yoshida [24] estimated the stress and strain paths during the bulge test, in case of in-plane anisotropic materials, using finite element analysis. He concludes that the stress path at the pole of the cap deviates from equibiaxial between 1–5%, depending on the degree of anisotropy of the materials. Also, he observed that the deviation from unity of the ratio between the curvature radii of the cap along the rolling and the transverse directions is less than 0.4%, for equivalent plastic strains up to 0.6, and less than 2%, for equivalent plastic strains up to 1.0. However, these results only concern materials with relatively low anisotropy in the sheet plane.

The current work presents a numerical study on the circular bulge test of metal sheets, performed with the *DD3IMP* in-house finite element code [25–27]. It examines the geometry and the stress and strain distributions near the pole of the cap. This analysis also concerns the relationship between stress and strain paths. Materials with anisotropy in the sheet plane are particularly considered. The methodology for the experimental determination of the stress *vs.* strain curve of metal sheets and associated errors is also analysed. The Hill'48 criterion [28] and the Swift law [29] are used due to their simplicity, but other constitutive models are also tested.

2. Numerical modelling and analysis

In this section, the numerical model of the circular bulge test is defined and the methodology for the evaluation of the biaxial stress *vs.* strain curve is described.

2.1. Modelling

The geometry of the tools considered in the test is schematically shown in Fig. 1, where $R_M = 75$ mm is the die radius, $R_1 = 13$ mm is the die profile radius, $R_D = 95$ mm is the radius of the central part of the drawbead and $R_S = 100$ mm is the initial blank radius of the circular sheet. This geometry was built based on the experimental bulge test used by Santos et al. [30]. The tools were described using Bézier surfaces, considering only one quarter of the geometry due to the material and geometrical symmetry conditions. However, in order to simplify the analysis, the drawbead geometry was neglected and its effect was replaced by a boundary condition imposing radial displacement restrictions on the nodes placed at a distance equal to R_D from the centre of the circular sheet [13]. The contact with friction was described by the Coulomb law with a friction coefficient of 0.02 [31]. The numerical simulations were carried out with the *DD3IMP* in-house code [25–27] assuming an incremental increase of the pressure applied to the sheet inner surface. The blank sheet, 1 mm thick, was discretized with linear 8-node solid elements, using two layers of elements through the thickness. More details about the spatial discretization adopted are given in [32,33].

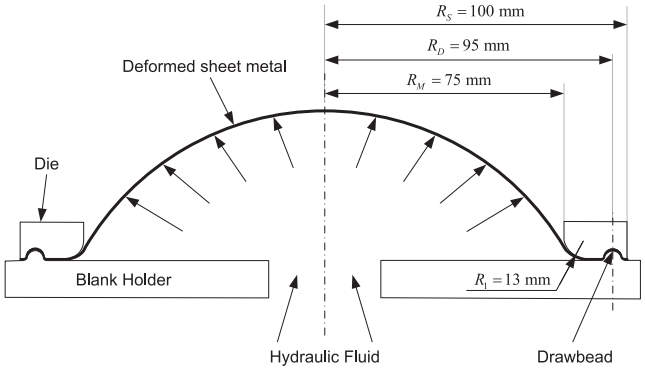

Fig. 1. Bulge test, with the identification of the principal dimensions of the tool according to Santos et al. [30].

The constitutive model adopted for the finite element analysis assumes that: (i) the elastic behaviour is isotropic and described by the generalised Hooke's law (with the value of the Young's modulus, $E = 210$ GPa, and the Poisson's ratio, $\nu = 0.30$, in all cases); (ii) the plastic behaviour is described by the orthotropic Hill'48, Drucker + L or CB2001 yield criteria and the hardening model by the Swift or the Voce isotropic laws.

The Hill'48 yield surface is described by the equation [28]:

$$F(\sigma_{yy} - \sigma_{zz})^2 + G(\sigma_{zz} - \sigma_{xx})^2 + H(\sigma_{xx} - \sigma_{yy})^2 + 2L\tau_{yz}^2 + 2M\tau_{xz}^2 + 2N\tau_{xy}^2 = Y^2, \quad (1)$$

where σ_{xx}, σ_{yy}, σ_{zz}, τ_{xy}, τ_{xz} and τ_{yz} are the components of the Cauchy stress tensor, defined in the principal axes of orthotropy, and F, G, H, L, M and N are the material parameters describing the anisotropy of the metal sheet. Y represents the yield stress and its evolution during deformation $Y = f(\bar{\varepsilon}^p)$.

The Hill'48 yield criterion was chosen because of its simplicity, but its lack of flexibility does not allow it to correctly describe some anisotropic behaviours, including those designated by Banabic as 'first and second order anomalous' behaviours [34]. In this context, the Drucker + L and the CB2001 criteria were also chosen due to their degree of flexibility.

The Drucker + L and the CB2001 yield criteria [35] are extensions of the Drucker isotropic yield criterion [36]. The Drucker + L yield criterion is described by the equation:

$$\left[\frac{1}{2}\mathrm{tr}(\mathbf{s}^2)\right]^3 - c\left[\frac{1}{3}\mathrm{tr}(\mathbf{s}^3)\right]^2 = 27\left(\frac{Y}{3}\right)^6, \quad (2)$$

where tr(**s**) is the trace of the stress tensor **s**, resulting from the linear transformation of the Cauchy stress tensor, **σ**, and c is a weighting isotropy parameter, ranging between $-27/8$ and $9/4$, to ensure the convexity of the yield surface. When c equals zero, this criterion coincides with the Hill'48 yield criterion. The **s** stress tensor is given by:

$$\mathbf{s} = \mathbf{L}\colon \boldsymbol{\sigma}, \quad (3)$$

where **L** is the linear transformation operator proposed by Barlat et al. [37]:

$$\mathbf{L} = \begin{bmatrix} (C_2 + C_3)/3 & -C_3/3 & -C_2/3 & 0 & 0 & 0 \\ -C_3/3 & (C_3 + C_1)/3 & -C_1/3 & 0 & 0 & 0 \\ -C_2/3 & -C_1/3 & (C_1 + C_2)/3 & 0 & 0 & 0 \\ 0 & 0 & 0 & C_4 & 0 & 0 \\ 0 & 0 & 0 & 0 & C_5 & 0 \\ 0 & 0 & 0 & 0 & 0 & C_6 \end{bmatrix}, \quad (4)$$

in which C_i, with $i = 1, \ldots, 6$, are the anisotropy parameters; $C_1 = C_2 = C_3 = C_4 = C_5 = C_6$ for the full isotropy condition. This yield criterion includes one more parameter, the parameter c, when compared to Hill'48 yield criterion, thus being more flexible. So, when the parameter c is not zero, Hill'48 criterion cannot fully describe the behaviour of a material that follows the Drucker + L criterion.

The CB2001 yield criterion is given by the equation:

$$(J_2^0)^3 - c(J_3^0)^2 = 27\left(\frac{Y}{3}\right)^6, \quad (5)$$

where J_2^0 and $J^0{}_3$ are the second and third generalised invariants of the Cauchy stress tensor:

$$
\begin{aligned}
J_2^0 &= \frac{a_1}{6}(\sigma_{xx}-\sigma_{yy})^2+\frac{a_2}{6}(\sigma_{yy}-\sigma_{zz})^2+\frac{a_3}{6}(\sigma_{xx}-\sigma_{zz})^2\\
&\quad + a_4\tau_{xy}^2+a_5\tau_{xz}^2+a_6\tau_{yz}^2\\
J_3^0 &= \frac{1}{27}(b_1+b_2)\sigma_{xx}^3+\frac{1}{27}(b_3+b_4)\sigma_{yy}^3\\
&\quad + \frac{1}{27}[2(b_1+b_4)-b_2-b_3]\sigma_{zz}^3\\
&\quad - \frac{1}{9}(b_1\sigma_{yy}+b_2\sigma_{zz})\sigma_{xx}^2-\frac{1}{9}(b_3\sigma_{zz}+b_4\sigma_{xx})\sigma_{yy}^2\\
&\quad - \frac{1}{9}[(b_1-b_2+b_4)\sigma_{xx}+(b_1-b_3+b_4)\sigma_{yy}]\sigma_{zz}^2\\
&\quad + \frac{2}{9}(b_1+b_4)\sigma_{xx}\sigma_{yy}\sigma_{zz}\\
&\quad - \frac{\tau_{xz}^2}{3}[2b_9\sigma_{yy}-b_8\sigma_{zz}-(2b_9-b_8)\sigma_{xx}]\\
&\quad - \frac{\tau_{xy}^2}{3}[2b_{10}\sigma_{zz}-b_5\sigma_{yy}-(2b_{10}-b_5)\sigma_{xx}]\\
&\quad - \frac{\tau_{yz}^2}{3}[(b_6+b_7)\sigma_{xx}-b_6\sigma_{yy}-b_7\sigma_{zz}]+2b_{11}\tau_{xy}\tau_{yz}\tau_{xz},
\end{aligned}
\tag{6}
$$

where a_1, …, a_6 and b_1, …, b_{11} are the anisotropy parameters; the full isotropy condition is attained when the values of a_k and b_k parameters are equal and $-3.375 \le c \le 2.25$.

The Swift isotropic hardening law [29] is defined by the equation:

$$Y = K(\varepsilon_0+\bar{\varepsilon}^p)^n, \tag{7}$$

where $\bar{\varepsilon}^p$ is the equivalent plastic strain and K, ε_0 and n are the material parameters. The initial yield stress, Y_0, can be written as a function of K, ε_0 and n, as follows: $Y_0 = K\varepsilon_0{}^n$. The Voce law [38] can be written as:

$$Y = Y_{sat} - R_{sat}\exp(-C_Y\bar{\varepsilon}^p), \tag{8}$$

where Y_{sat}, R_{sat} and C_Y are materials parameters; the yield stress is $Y_0 = Y_{sat}$-R_{sat}.

The Swift law enables the description of an increasing hardening while the Voce law takes into account the occurrence of flow stress saturation; both are behaviours often observed in some metals and alloys.

2.2. Analyses

The analysis of the stress state near the pole of the metal sheet during the bulge test, when using circular dies, can be performed with the aid of the membrane theory [39], as long as a small ratio between the sheet thickness and the die diameter is fulfilled. The typical values suggested for this ratio are lower than 1/50 [9,40]. Standard ISO 16808:2014 [21] recommends this ratio to be equal to or lower than 1/33. Under these conditions the bending stress can be neglected, and assuming that the thickness stress σ_3 ($=\sigma_Z$) is equal to zero, a relationship between the principal stresses at the pole, the pressure and the geometry of the cap is given by:

$$\frac{\sigma_1}{\rho_1}+\frac{\sigma_2}{\rho_2}=\frac{p}{t}, \tag{9}$$

where σ_1 and σ_2 are the principal stresses in the sheet surface (assuming that the principal stress axes, O123, and the orthotropy axes, O*xyz*, coincide), ρ_1 and ρ_2 are the radii of curvature, at half thickness, in the O*xz* and O*yz* planes, respectively, p is the hydraulic pressure and t is the sheet thickness.

Finally, in cases of circular die and isotropic or anisotropic materials such that, the anisotropy coefficients at 0 and 90° are equal ($r_0 = r_{90}$), the principal stresses in the sheet plane are also equal ($\sigma_1 = \sigma_2 = \sigma$), as well as the radii of curvature ($\rho_1 = \rho_2 = \rho$), which simplifies Eq. (9) as follows:

$$\sigma = \frac{p\rho}{2t}. \tag{10}$$

And so, this equation is sufficient to determine the principal stresses in the sheet plane ($\sigma_1 = \sigma_2 = \sigma$), without requiring any additional equation. This assumption is adopted in the ISO 16808:2014 [21] standard to enable the definition of the biaxial stress.

In order to experimentally determine the biaxial stress *vs.* strain curve, the evolution of the variables in Eqs. (9) or (10) needs to be assessed during the test. The sheet thickness at the pole of the cap, t, is determined based on the knowledge of the initial thickness of the sheet, t_0, and the thickness strain, ε_3, through the following equation:

$$t = t_0\exp(-\varepsilon_3), \tag{11}$$

where the principal strain, ε_3, is obtained from the principal strains in the sheet plane, ε_1 and ε_2, at the pole of the cap, based on the condition of volume constancy during the plastic deformation:

$$\varepsilon_3 = -(\varepsilon_1+\varepsilon_2). \tag{12}$$

Given that the radius of curvature is experimentally evaluated on the external surface of the cap, its correction is performed based on the following equation [41]:

$$\rho = \rho_{ext} - \frac{t}{2}, \tag{13}$$

where ρ is the radius of curvature at the half thickness of the cap, and ρ_{ext} is the radius of curvature of the external surface of the cap.

Since the total strain presents two additive components, elastic and plastic, the elastic strain components, ε_1^e and ε_2^e, can be removed from the measured strains, ε_1 and ε_2. Assuming isotropic elastic behaviour, the generalised Hooke's law, gives the elastic strain components as ($\sigma_3 = 0$):

$$
\begin{cases}
\varepsilon_1^e = \frac{1}{E}(\sigma_1-\nu\sigma_2)\\
\varepsilon_2^e = \frac{1}{E}(\sigma_2-\nu\sigma_1)
\end{cases}.
\tag{14}
$$

In order to determine the biaxial stress *vs.* strain curves, the analysis of the numerical simulation results was performed at various stages during the test, using step-wise measurements, as in typical experimental analysis. The evaluation of the surface radius of curvature, ρ_{ext}, at the pole of the cap is performed using *NXT Defect Evaluator* code [42]. This software allows the evaluation of surface curvature based on the coordinates of points located on the same meridian plane. The surface radius of curvature, ρ_{ext}, was analysed for both O*xz* and O*yz* planes. The radius of curvature at half thickness, ρ, is determined using Eq. (13). At each stage, the principal strains in the sheet plane were determined by the direct measurement at the pole of the cap, which is comparable to the experimental procedure using the digital image correlation technique (DIC).

3. Geometry of the cap, stress and strain distribution and their paths

The study in this section focuses on materials whose behaviour is described by the Hill'48 criterion and the isotropic Swift hardening law. The analysis of the distributions, near the pole of the cap of the bulge test, of variables such as the surface radius of curvature, the sheet thickness, the principal and equivalent stresses and strains as well as the stress and strain paths is performed. The analysis mainly focuses on in-plane anisotropic materials with $r_0 \neq r_{90}$, for which there remains a lack of knowledge about these aspects. In fact, in case of in-plane isotropic materials, most of these issues have already been analysed (see for example [22]), in view of their relative simplicity related to the geometrical and material symmetry. Also, the materials of the current study with $r_0 = r_{90} \neq r_{45}$ show identical behaviour along the O*x* and O*y* axes, as expected due to the symmetry of the yield surface in the (σ_{xx}; σ_{yy}) plane and the geometrical symmetry of the circular bulge test. That is why the analysis in this section deals primarily with materials such that $r_0 \neq r_{90}$.

Table 1
Designation of the materials and the respective parameters of the Hill'48 criterion.

Designation	Parameters of the Hill'48 Criterion				
	F	*G*	*H*	*L*=*M*	*N*
Materials with $r_0=r_{45}=r_{90}$					
0.7_0.7_0.7	0.588	0.588	0.412	1.500	1.412
1_1_1	0.500	0.500	0.500	1.500	1.500
2_2_2	0.333	0.333	0.667	1.500	1.667
3_3_3	0.250	0.250	0.750	1.500	1.750
Materials with $r_0=r_{90}\neq r_{45}$					
0.6_3_0.6	0.625	0.625	0.375	1.500	4.375
3_0.6_3	0.250	0.250	0.750	1.500	0.550
1.5_3_1.5	0.400	0.400	0.600	1.500	2.800
3_1.5_3	0.250	0.250	0.750	1.500	1.000
Materials with $r_0\neq r_{90}$					
0.6_0.7_0.8	0.469	0.625	0.375	1.500	1.313
0.6_1.8_3	0.125	0.625	0.375	1.500	1.725
1.5_2.25_3	0.200	0.400	0.600	1.500	1.650
1.5_2.75_4	0.150	0.400	0.600	1.500	1.788
0.5_2.25_4	0.083	0.667	0.333	1.500	2.063
1.5_3_3	0.200	0.400	0.600	1.500	2.100
1_2.25_3.5	0.143	0.500	0.500	1.500	1.768

3.1. Sheet materials

Table 1 shows the parameters of the Hill'48 criterion of the materials under study and the respective designation. The condition $G+H=1$ was used for the parameters of the Hill'48 criterion, *i.e.* it is assumed that the hardening curve $Y(\bar{\varepsilon}^p)$ corresponds to the stress *vs.* plastic strain curve under uniaxial tensile test along the O*x* axis [43]. The designation A_B_C corresponds to a material with anisotropy coefficients r_α in the sheet plane, such that: r_0=A, r_{45}=B and r_{90}=C (α is the angle between the tensile direction and the rolling direction, RD parallel to O*x*). The selected materials for this study display three different types of behaviour in the sheet plane: (i) isotropy: $r_0=r_{45}=r_{90}$; (ii) anisotropy with: $r_0=r_{90}\neq r_{45}$; (iii) anisotropy with: $r_0\neq r_{90}$. Fig. 2 shows the evolution of the anisotropy coefficient, r_α, in the sheet plane for the materials with in-plane anisotropy.

Figs. 3 and 4 show the normalized initial yield surfaces in the plane ($\sigma_{xx}/\sigma^0{}_0$; $\sigma_{yy}/\sigma^0{}_0$), of the materials with $r_0=r_{90}=r_{45}$ and $r_0=r_{90}\neq r_{45}$ (Fig. 3), and with $r_0\neq r_{90}$ (Fig. 4). In both figures, the dashed-dotted grey straight lines correspond to the condition $\sigma_{yy}=\sigma_{xx}$; the remaining straight lines in Fig. 4 indicate the major axes of the ellipses. The yield surfaces in the plane ($\sigma_{xx}/\sigma^0{}_0$; $\sigma_{yy}/\sigma^0{}_0$) are coincident in case of the materials: 3_3_3, 3_1.5_3 and 3_0.6_3 (see Fig. 3); 1.5_2.25_3 and 1.5_3_3 (see Fig. 4). The yield surfaces of the materials 0.5_2.25_4 and 0.6_1.8_3, for which $r_0<1$ and $r_{90}>1$, have their major axes with higher slope than those of the remaining materials; moreover, the axes of the yield surfaces for materials 0.6_0.7_0.8 and 1.5_2.75_4 are collinear (Fig. 4). In summary, the choice of materials is focused on: (i) in-plane isotropic materials, with different anisotropy coefficients and, consequently, several shapes of the yield surface near the equibiaxial region (different ratios between the major and minor axes of the ellipse) and (ii) in-plane anisotropic materials with different ratios between the major and minor axes of the ellipse as well as different orientations of these axes.

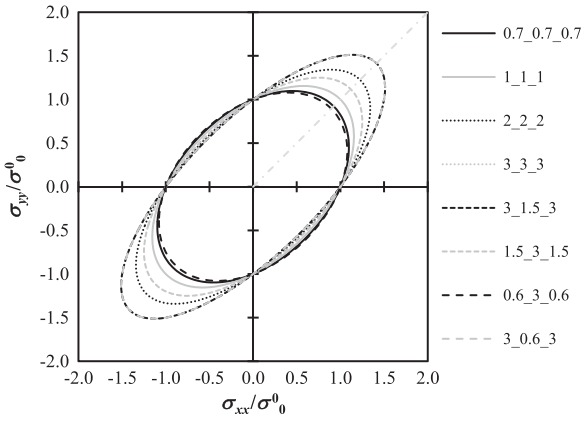

Fig. 3. Normalized initial yield surfaces in the plane ($\sigma_{xx}/\sigma^0{}_0$; $\sigma_{yy}/\sigma^0{}_0$) of the materials with $r_0=r_{90}=r_{45}$ and $r_0=r_{90}\neq r_{45}$.

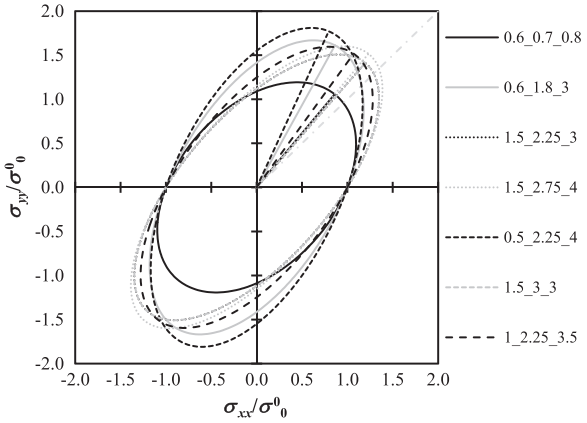

Fig. 4. Normalized initial yield surfaces in the plane ($\sigma_{xx}/\sigma^0{}_0$; $\sigma_{yy}/\sigma^0{}_0$) of the materials with $r_0\neq r_{90}$.

The parameters of the Swift hardening law, for the materials studied in the next sections, are shown in Table 2. Simulations were performed for all the materials in Table 1 with the work hardening coefficient, *n*, equal to 0.20 (Table 2). The hardening laws with work hardening coefficients, *n*, equal to 0.10 and 0.35 were only used for simulations of

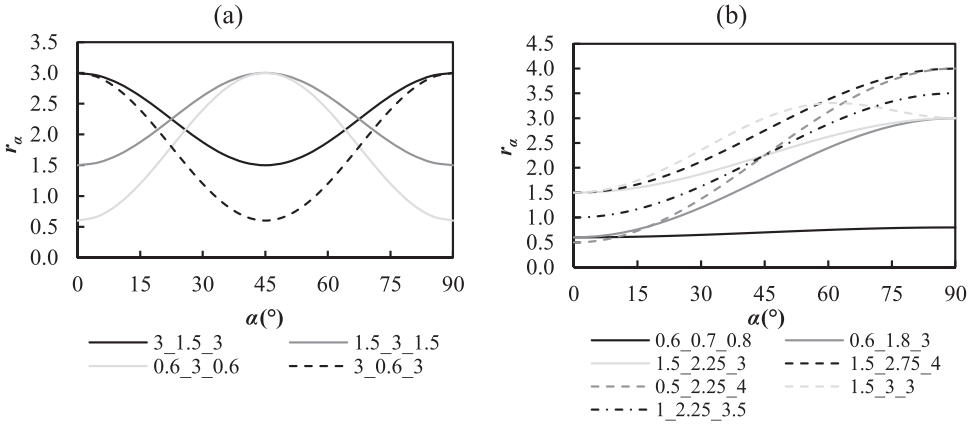

Fig. 2. Distribution of r_α in the sheet plane, for materials with in-plane anisotropy: (a) $r_0=r_{90}\neq r_{45}$; (b) $r_0\neq r_{90}$.

Table 2
Parameters of the Swift hardening law.

Materials	Parameters of the Swift law			
	Y_0 [MPa]	K [MPa]	ε_0	n
200_0.10	200	339.73	0.005	0.10
200_0.20	200	577.08	0.005	0.20
200_0.35	200	1277.59	0.005	0.35

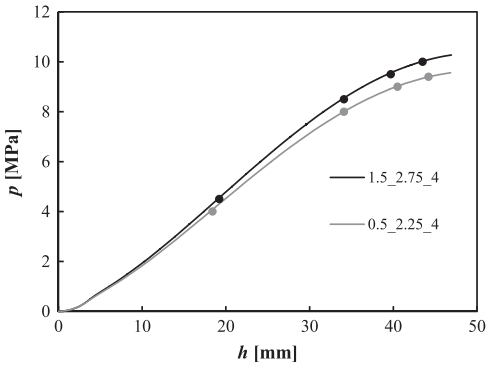

Fig. 5. Evolution of the pressure, p, with the pole height, h, for materials 1.5_2.75_4 and 0.5_2.25_4. The dots concern the pressure values on which the analysis is focused: 4.5, 8.5, 9.5 and 10 MPa, for the material 1.5_2.75_4, and 4, 8, 9 and 9.4 MPa, for the material 0.5_2.25_4. The hardening coefficient of both materials is $n=0.20$.

the materials 0.6_0.7_0.8, 1.5_2.75_4 and 0.5_2.25_4 (Table 1).

The materials with strong anisotropy in the sheet plane, 1.5_2.75_4 and 0.5_2.25_4, and with hardening coefficient, $n=0.20$, were chosen to illustrate the general behaviour, that is not only at the pole of the cap, but also at distant points. Fig. 5 shows the evolution of pressure with the pole height for these materials and the instants of the bulge test under analysis. These correspond to four pressure values during the tests, marked in the figure with dots, which corresponds to: (i) material 1.5_2.75_4 with pressure values of 4.5, 8.5, 9.5 and 10 MPa (corresponding to the Hill'48 equivalent strains equal to 0.066, 0.231, 0.329 and 0.421 at the pole of the cap, respectively); and (ii) material 0.5_2.25_4 with pressure values of 4, 8, 9 and 9.4 MPa (corresponding to the Hill'48 equivalent strains equal to 0.059, 0.229, 0.336 and 0.421 at the pole of the cap, respectively).

3.2. Contour of the cap and thickness distribution

Fig. 6 shows the contours of the cap, *i.e.* the vertical position of each point, z, as a function of the distance from the centre, d, along the Ox and Oy axes, for the materials 1.5_2.75_4 (Fig. 6(a)) and 0.5_2.25_4 (Fig. 6(b)) and the pressure values previously mentioned (see Fig. 5). Whatever the pressure value, the Ox and Oy profiles coincide, from the centre to the edge of the cap (Fig. 6). This means that the radii of curvature at the pole of the cap does not depend on the measuring axis, Ox or Oy, which was also confirmed by the evaluation of both radii of curvature.

Fig. 7 shows the evolution of the thickness as a function of the distance to the centre, d, along the Ox and Oy axes, for the materials 1.5_2.75_4 (Fig. 7(a)) and 0.5_2.25_4 (Fig. 7(b)), at the pressure values previously mentioned (see Fig. 5). As for the profiles, the thickness distributions are almost coincident for the axes Ox and Oy at the two first steps analysed, but some differences are noticeable for the two higher pressure values, mainly in case of the material 0.5_2.25_4. These differences in thicknesses occurs in this material for distances from the centre higher than about 20 mm, at the pressure equal to 9 MPa, and higher than at about 15 mm, at the pressure equal to 9.4 MPa.

In summary, the analysis of the surface shape of the deformed sheet showed that, regardless of the anisotropic material behaviour, the geometry of the cap has symmetry such that the radii of curvature at the pole of the cap are equal along the axes Ox and Oy ($\rho_1=\rho_2=\rho$), at each moment of the test, the same occurring for the sheet thickness. On the contrary, the principal stress and strain distributions are different along these axes, *i.e.* the stress and strain paths at the pole of the cap are always different from 1 ($\sigma_1 \neq \sigma_2$ and $\varepsilon_1 \neq \varepsilon_2$), as it will be seen in the next sections.

3.3. Stress and strain distributions

Figs. 8 and 9 show the distributions of the principal strains and stresses, parallel to the Ox and Oy directions, for the materials and pressure values as in Figs. 6 and 7 (see also Fig. 5). For a region around the pole of the cap, whose size decreases as the test progresses, the strain and stress components parallel (normal) to the Ox axis, at a given point on this axis, are equal to the corresponding normal (parallel) components to the Oy axis, for a point on this axis at the same distance from the centre of the cap. At a given pole height, the size of this region is smaller the greater the planar anisotropy of the material, as it can be concluded by comparing the results of materials 1.5_2.75_4 (Fig. 8) and 0.5_2.25_4 (Fig. 9).

Figs. 10 and 11 show the distributions of the Hill'48 equivalent strains and stresses, along the Ox and Oy directions, for the same materials and pressure values as in Figs. 6–9 (see also Fig. 5). Following the trends in Figs. 8 and 9, the equivalent strains and stresses are equal along both orthotropic axes, in a region around the pole. This region becomes smaller with the increase of the pole height but, even near the end of the test, its size is about 10 mm, for the material 0.5_2.25_4, and

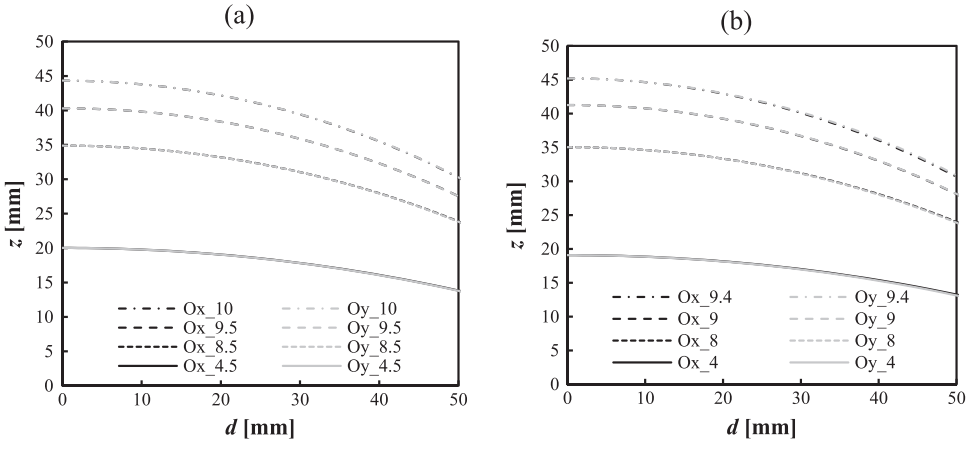

Fig. 6. Contours of the cap at the four pressure values indicated in Fig. 5, *i.e.* vertical position, z, as a function of the distance to the centre of the cap, d, along the Ox and Oy axes, for the materials: (a) 1.5_2.75_4; (b) 0.5_2.25_4. The hardening coefficient of both materials is $n=0.20$.

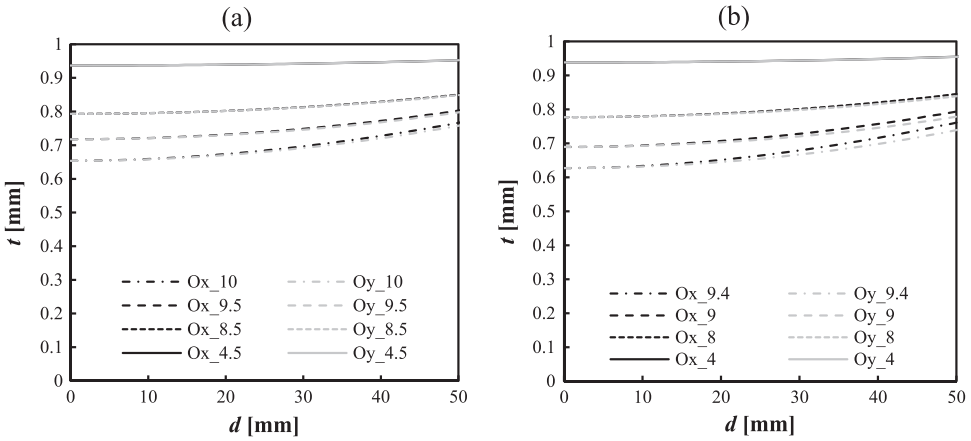

Fig. 7. Evolution of the sheet thickness, t, with the distance from the centre of the cap, d, along the Ox and Oy axes, at the four pressure values indicated in Fig. 5, for the materials: (a) 1.5_2.75_4; (b) 0.5_2.25_4. The hardening coefficient of both material is $n=0.20$.

higher for the material 1.5_2.75_4, in case of equivalent strain, and covers almost the entire diameter of the die, for both materials in the case of equivalent stress.

3.4. Stress and strain path evolutions at the pole

Based on results such as in Figs. 8 and 9, Fig. 12 present the stress (Fig. 12(a)) and strain (Fig. 12(b)) paths observed at the pole of the cap, for in-plane anisotropic materials with hardening coefficient, $n=0.20$, showing that the stress paths are nearly unchanged during the bulge test, although with minor variations. However, noticeable decreasing of the strain path occurs during the test, in most cases. In fact, a small variation in the stress path can give rise to a relatively larger amplitude of variation of the strain path, which is represented by the normal to the yield surface. The amplitude of variation of the strain path during each test is always inferior to 5%, whatever the material (the maximum difference occurs for the material 0.5_2.25_4).

The stress and strain paths are also influenced by the value of the hardening coefficient of the material. Fig. 13 allows comparing the materials 0.6_0.7_0.8, 1.5_2.75_4 and 0.5_2.25_4, with $n=0.10$, 0.20 and 0.35 concerning the stress and strain paths (Fig. 13(a) and (b), respectively). The stress paths are almost unchanged during the test, and nearly close to each other for a given value of the hardening coefficient. Nevertheless, the small variations that occur in the stress path are enough to cause relatively large variations in the strain path (in agreement with the associated flow rule), which decreases during the test, *i.e.* deviates from the equibiaxial (except for the material 0.5_2.25_4, with $n=0.10$), as for results in Fig. 12. It can be observed that in general the strain path is lower for higher values of the hardening coefficient.

3.5. Final remarks

As partial conclusions, it can be stated that, as for the materials with $r_0=r_{90}$, also for the materials with $r_0\neq r_{90}$ the geometry of the cap is similar along both orthotropic axes in the sheet plane, with respect to the profile and the thickness of the sheet, which is imposed by the geometrical constrains of the bulge test with circular die. The results show that this type of symmetry can be achieved even though the stress and strain paths in the pole region are away from the biaxial symmetry. The inability to impose equibiaxial stress and strain paths simultaneously, in case of materials with $r_0\neq r_{90}$, arises from the normality condition, *i.e.* the associated flow rule with the yield surface as plastic potential, which in case of the Hill'48 criterion leads to the following equation (under the assumptions of coincidence of the coordinate systems of principal stress, O123, and orthotropy, Oxyz, and that $\sigma_3=\sigma_z=0$):

$$\frac{d\varepsilon_2}{d\varepsilon_1}=\frac{-H+\frac{\sigma_2}{\sigma_1}(F+H)}{(G+H)-\frac{\sigma_2}{\sigma_1}H}. \tag{15}$$

This equation can also be written as a function of the anisotropy coefficients, r_0 and r_{90}:

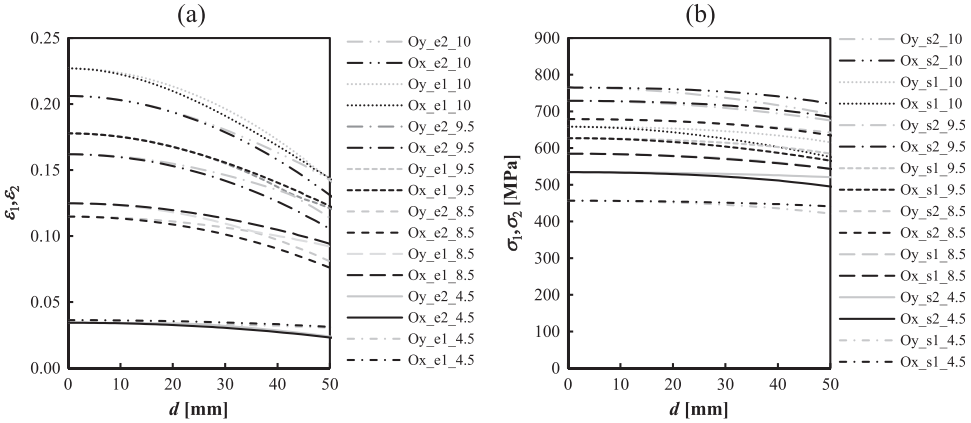

Fig. 8. Evolution of the (a) principal strains and (b) principal stresses, with the distance from the centre of the cap, d, along the axes Ox and Oy of the sheet, for the material 1.5_2.75_4 at the four pressure values indicated in Fig. 5. The hardening coefficient of the material is $n=0.20$. The designation in figures can be read as for the example(s): Ox_e1_10 (Oy_s2_4.5), in which Ox (Oy) indicates the axis for measuring the distance d; e1 (s2) is the strain (stress) value parallel to the Ox (Oy) axis; and 10 (4.5) is the pressure value [MPa].

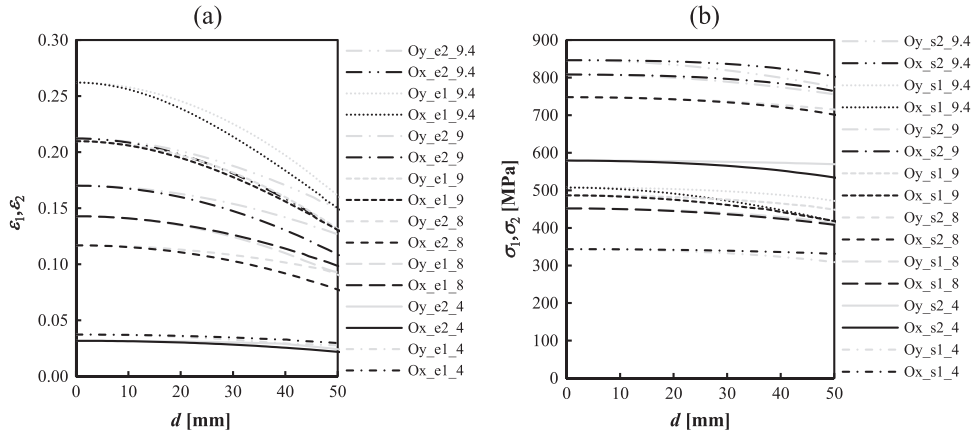

Fig. 9. Evolution of the (a) principal strains and (b) principal stresses, with the distance to the centre of the cap, *d*, for the material 0.5_2.25_4 at the four pressure values indicated in Fig. 5. The hardening coefficient of the material is $n=0.20$. The designations are as indicated in Fig. 8.

$$\frac{d\varepsilon_2}{d\varepsilon_1} = \frac{-1 + \frac{\sigma_2}{\sigma_1}\left(\frac{1}{r_{90}} + 1\right)}{\left(\frac{1}{r_0} + 1\right) - \frac{\sigma_2}{\sigma_1}}. \tag{16}$$

This equation shows that, for materials with $r_0 < r_{90}$ as those studied in this work, when the stress path is equal to 1, the strain path is lower than 1, and when the strain path is equal to 1, the stress path is higher than 1 (the opposite occurs when $r_0 > r_{90}$). In fact, the observed stress and strain paths are between these two cases, as schematized in Fig. 14. The way this behaviour influences the evaluation of the biaxial stress-strain curve will be analysed in the next section.

4. Biaxial stress-strain curve

The determination of the biaxial stress *vs.* strain curve, of materials whose behaviour is described by the Hill'48 yield criterion, is tested under conditions similar to those experimentally performed. The stress at the pole of the cap is determined using the simplified equation of the membrane theory (Eq. (10)), as recommended by ISO 16808:2014 [21]. This standard also recommends the measuring of both principal strains in the sheet plane, which requires the use of optical measurement systems; but when using tactile systems only one principal strain value is measured. Both cases are tested in this section, using the strains numerically measured, at the pole of the cap.

4.1. Introduction

The assumption of isotropy for determining the equivalent stress (*i.e.* the use of Eq. (10) for the stress evaluation), can be interpreted as the finding of the value of equivalent stress generating a von Mises yield surface that intercepts (or is tangent to) the yield surface of the anisotropic material, at the point corresponding to the stress path followed during the bulge test of the anisotropic material. Examples are shown in the Fig. 15, for the Hill'48 materials with in-plane isotropy, 3_3_3 (Fig. 15(a)) and anisotropy 0.5_2.25_4 (Fig. 15(b)). In Fig. 15(b), the marked stress path is the average of those observed during the bulge test (see in Fig. 12(a) the case of material 0.5_2.25_4).

The Hill'48 and the von Mises equivalent stresses can be written as follows (in case of the Hill'48, assuming the coincidence of the coordinate systems of principal stress, O123, and orthotropy, O*xyz*):

$$\bar{\sigma} = \sqrt{(G+H)\sigma_1^2 + (F+H)\sigma_2^2 - 2H\sigma_1\sigma_2}, \tag{17}$$

$$\bar{\sigma} = \sqrt{\sigma_1^2 + \sigma_2^2 - \sigma_1\sigma_2}, \tag{18}$$

The Hill'48 material parameters in Table 1 follow the condition $G+H=1$, which means that the hardening laws (Table 2) are only comparable with the stress *vs.* strain curves in tension along the O*x* axis. The constitutive parameters in Tables 1 and 2 can be recalculated, *i.e.* converted into equivalent sets of constitutive parameters [41], so that the Hill'48 equivalent stress, $\bar{\sigma}_{\text{Hill'48}}$ (= $\bar{\sigma}$ in Eq. (17)), becomes equal to the von Mises stress, $\bar{\sigma}_{\text{vM}}$ (= $\bar{\sigma}$ in Eq. (18)), as shown in Tables 3 and 4. This makes the hardening laws associated with the Hill'48 criterion comparable to the biaxial stress *vs.* strain curves of the bulge test

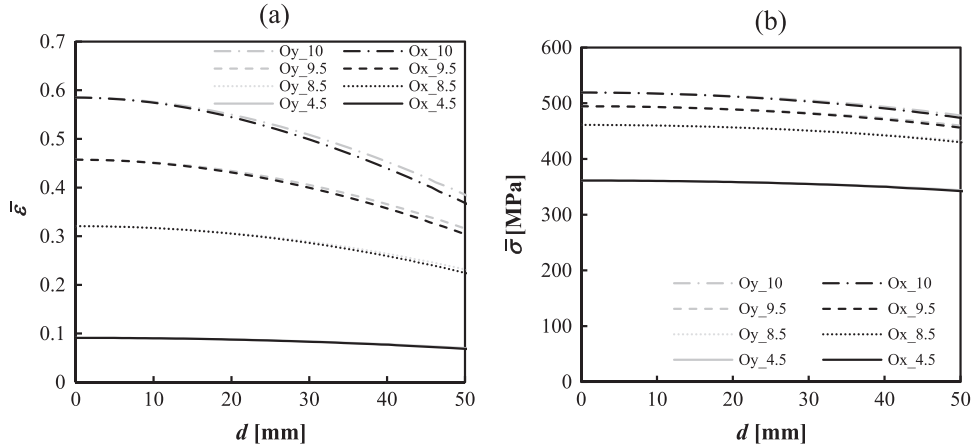

Fig. 10. Evolution of the (a) equivalent strain and (b) equivalent stress with the distance to the centre of the cap, *d*, along the O*x* and O*y* axes, for the material 1.5_2.75_4 at the four pressure values indicated in Fig. 5. The hardening coefficient of the material is $n=0.20$.

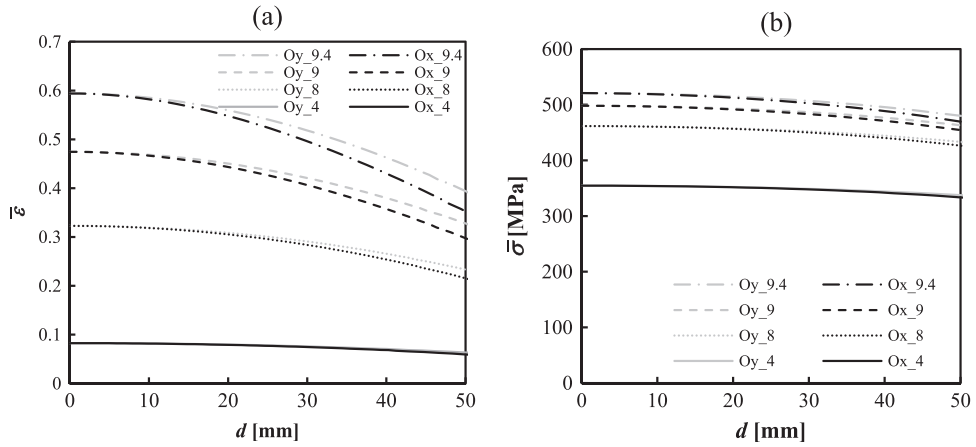

Fig. 11. Evolution of (a) equivalent strain and (b) equivalent stress with the distance to the centre of the cap, *d*, along the O*x* and O*y* axes, for the material 0.5_2.25_4 at the four pressure values indicated in Fig. 5. The hardening coefficient of the material is $n=0.20$.

determined, without taking into account the material anisotropy. The determination of $\bar{\sigma}_{vM}/\bar{\sigma}_{Hill'48}=\sqrt{k}$, with:

$$k=\frac{1+(\sigma_2/\sigma_1)^2-(\sigma_2/\sigma_1)}{(G+H)+(F+H)(\sigma_2/\sigma_1)^2-2H(\sigma_2/\sigma_1)}, \tag{19}$$

requires the knowledge of the stress path. In case of in-plane isotropic materials and materials with $r_0=r_{90}\neq r_{45}$, this does not involve any difficulty, given that σ_2/σ_1 is always equal to 1, at the pole of the cap. In case of materials with $r_0\neq r_{90}$, the stress path at the pole is different from 1 ($\sigma_2\neq\sigma_1$), usually unknown from the experimental point of view and depends on the material anisotropy and work hardening coefficient. For each of these materials, the average value of the stress path along the test, obtained from Figs. 12(a) and 13(a), was used for determining the constitutive parameters in Tables 3 and 4.

The relationships that allow the equivalence between the sets of parameters were previously discussed in [43] and, in the current case, are based on the factor $\sqrt{k}$ so that Eqs. (17) and (18) lead to the same value of equivalent stress. Therefore, the knowledge of the $\sqrt{k}$ factor allows defining the new parameters for the Swift law as:

$$n^*=n;\ K^*=K(\sqrt{k})^{n+1};\ \varepsilon_0^*=\varepsilon_0/\sqrt{k};\ Y_0^*=Y_0\sqrt{k}. \tag{20}$$

It should be mentioned that when using these new parameters for the Swift law, the mechanical behaviour of the materials presented in Tables 1 and 2 remains unchanged, if the parameters of the Hill'48 yield criterion are modified as follows [43]:

$$F^*=kF;\ G^*=kG;\ H^*=kH;\ L^*=kL;\ M^*=kM;\ N^*=kN. \tag{21}$$

The parameters without asterisk are those in Tables 1 and 2 and with asterisk are shown in Tables 3 and 4 (for convenience of the presentation, the asterisks are not indicated in Tables 3 and 4). Table 3 shows the hardening law and the Hill'48 criterion equivalent parameters of all materials in Table 1 and hardening coefficient $n=0.20$ (Table 2), and Table 4 the equivalent parameters of the three materials in Table 1 with $r_0\neq r_{90}$ and hardening coefficients 0.10 and 0.35 (Table 2). In both tables the respective stress paths and k values are also shown.

In Tables 3 and 4, the condition $F+G=1$ is observed for the materials with $r_0=r_{90}$, which means that the hardening curves are comparable to the equibiaxial stress *vs.* strain curves. For materials with $r_0\neq r_{90}$ the sum $(F+G)$ can deviate significantly from one, depending on the stress path observed during the bulge test, and the hardening curves are comparable to the biaxial stress *vs.* strain curves determined for the observed stress path.

In the next sections, the issues related with the errors associated with the assumption of isotropy and equibiaxial stress at the pole of the cap, under the context of the membrane theory (Eq. (10)), are analysed.

4.2. Materials with $r_0=r_{90}$

In case of in-plane isotropic materials and materials with $r_0=r_{90}\neq r_{45}$ (Table 3), the strain and stress paths at the pole of the cap are known *a priori*, and equal to 1. An equivalence is easily obtained between the Hill'48 and the von Mises criteria, for determining the equivalent stress: Eqs. (17) and (18) give the same result for all these materials ($\bar{\sigma}=\sigma_1=\sigma_2$, for both criteria). Consequently, the simplified equation of the membrane theory (Eq. (10)) allows to determine the

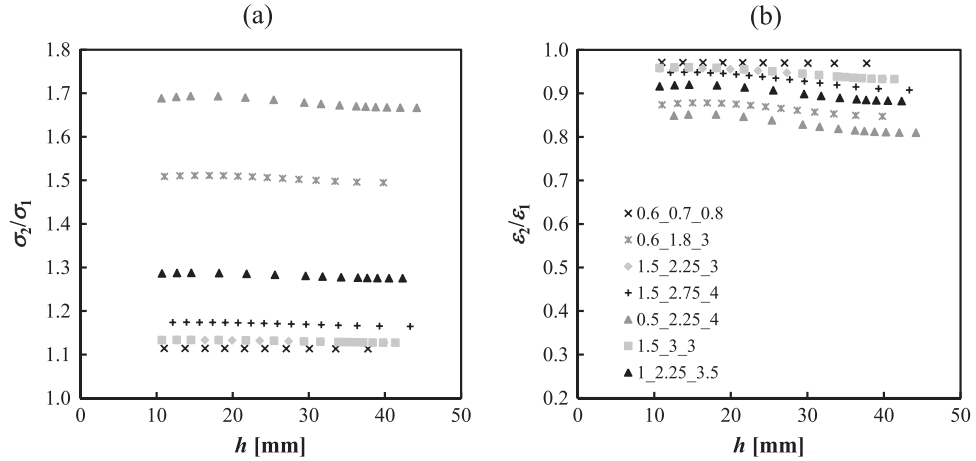

Fig. 12. Evolution of the: (a) stress paths and (b) strain paths, at the pole of the cap, during the test. These evolutions concern the materials with hardening coefficient equal to 0.20.

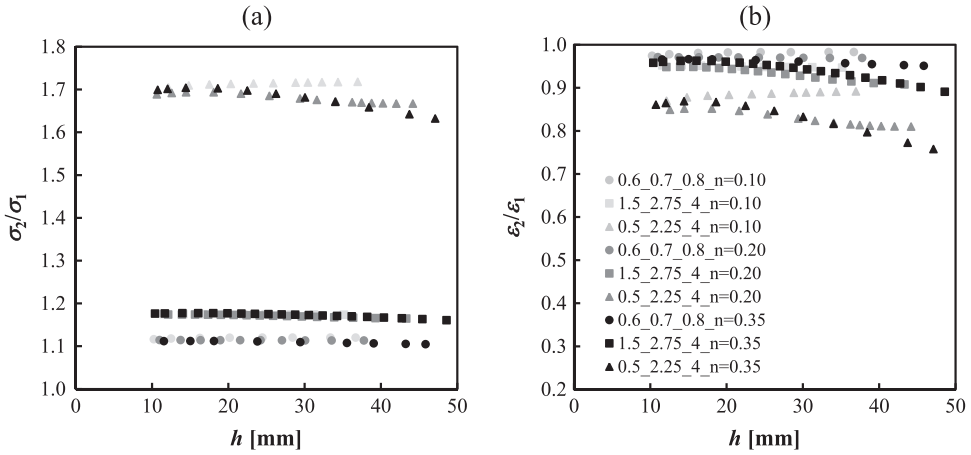

Fig. 13. Evolution of the: (a) stress paths and (b) strain paths, at the pole of the cap, during the test. These evolutions concern the materials 0.6_0.7_0.8, 1.5_2.75_4 and 0.5_2.25_4, with hardening coefficients equal to 0.10, 0.20 and 0.35.

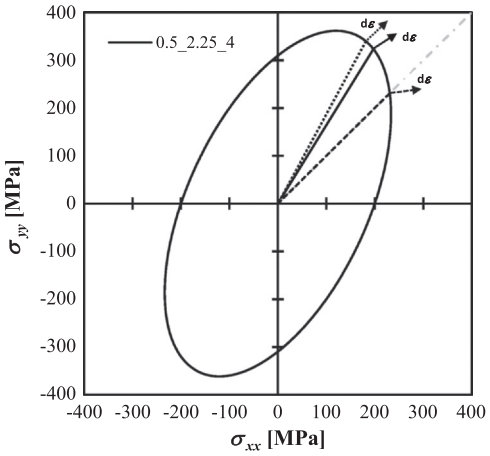

Fig. 14. Illustrative example, corresponding to the material 0.5_2.25_4 with $n=0.20$, showing the yield surface and the average of the observed values (see Fig. 12) of the stress and strain paths (solid lines), the stress and strain paths corresponding to equibiaxial stress path (dashed lines) and equibiaxial strain path (dotted lines).

stress $\sigma=\sigma_1=\sigma_2$, as recommended by ISO 16808:2014 [21].

Moreover, the equivalent plastic strain values are equal for both criteria, for the equibiaxial strain path. In fact, the equivalent plastic strains are given by the following equations for the Hill'48 and von Mises criteria (in case of the Hill'48, assuming the coincidence of the coordinate systems of principal stress, O123, and orthotropy, O*xyz*), respectively:

$$\bar{\varepsilon} = \sqrt{\frac{(F+H)\varepsilon_1^2 + (G+H)\varepsilon_2^2 + 2H\varepsilon_1\varepsilon_2}{FG+GH+HF}}, \tag{22}$$

$$\bar{\varepsilon} = \left(\frac{2}{\sqrt{3}}\right)\sqrt{\varepsilon_1^2 + \varepsilon_2^2 + \varepsilon_1\varepsilon_2}. \tag{23}$$

In case of von Mises criterion, Eq. (23) assumes the simplified formulation for the equibiaxial strain path ($\varepsilon_1 = \varepsilon_2 = \varepsilon$):

$$\bar{\varepsilon} = 2\varepsilon. \tag{24}$$

When $\varepsilon_1=\varepsilon_2$, Eqs. (22) and (24) give the same result for the equivalent plastic strain of these materials: $\bar{\varepsilon} = 2\varepsilon$. This is illustrated in Fig. 16 for the case of the material 3_3_3, which represents in the (ε_1; ε_2) plane the curves with equal equivalent plastic strain ($\bar{\varepsilon} = 1$), for the Hill'48 and von Mises criteria, showing that the curves are tangent for the equibiaxial strain path ($\varepsilon_1=\varepsilon_2$).

In summary, the biaxial stress *vs*. plastic strain and the hardening law curves must match, whatever the yield criteria used, Hill'48 or von Mises, for materials with $r_0=r_{90}$. That is, the use of the von Mises criterion for determining the biaxial stress *vs*. strain curve is fully justified for materials with $r_0=r_{90}$. From the experimental point of

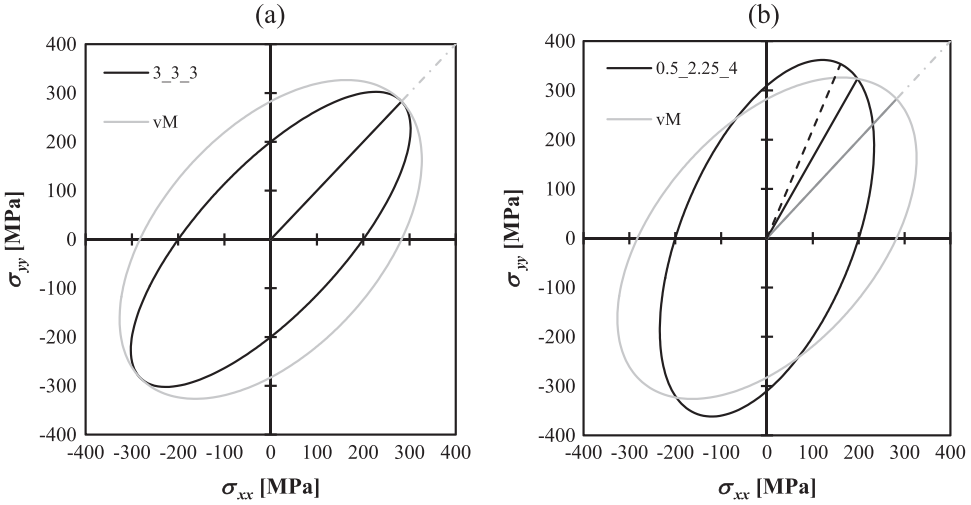

Fig. 15. Initial yield surfaces and the observed stress paths (black solid line) of the materials: (a) 3_3_3; (b) 0.5_2.25_4. The isotropic materials with equal equivalent stress are also indicated in each figure (vM). The bulge stress path at the pole (black solid lines) is equibiaxial, in case of (a), and is $\sigma_2/\sigma_1=1.678$, in case of (b). The black dashed and the grey solid lines in (b) represent the axis of the Hill'48 and the von Mises ellipses, respectively. The hardening coefficient of the materials is $n=0.20$.

Table 3
Constitutive parameters equivalent to those in Table 1 for the material 200_0.20 in Table 2. The average stress paths observed during the bulge test and the k value are also indicated.

Designation	Parameters of the Swift law			Parameters of the Hill'48 criterion						
	Y_0 [MPa]	K [MPa]	n	F	G	H	$L=M$	N	σ_2/σ_1	k
Materials with $r_0=r_{45}=r_{90}$										
0.7_0.7_0.7	184.43	523.59	0.20	0.500	0.500	0.350	1.201	1.200	1.000	0.850
1_1_1	200.00	577.08	0.20	0.500	0.500	0.500	1.500	1.500	1.000	1.000
2_2_2	245.07	736.46	0.20	0.500	0.500	1.002	2.252	2.503	1.000	1.502
3_3_3	282.84	874.69	0.20	0.500	0.500	1.500	3.000	3.500	1.000	2.000
Materials with $r_0=r_{90}\neq r_{45}$										
0.6_3_0.6	178.89	504.77	0.20	0.500	0.500	0.300	1.200	3.500	1.000	0.800
3_0.6_3	282.84	874.69	0.20	0.500	0.500	1.500	3.000	1.100	1.000	2.000
1.5_3_1.5	223.84	659.75	0.20	0.500	0.500	0.750	1.875	3.500	1.000	1.250
3_1.5_3	282.84	874.69	0.20	0.500	0.500	1.500	3.000	2.000	1.000	2.000
Materials with $r_0\neq r_{90}$										
0.6_0.7_0.8	192.87	552.47	0.20	0.436	0.581	0.349	1.395	1.221	1.114	0.930
0.6_1.8_3	264.83	808.29	0.20	0.219	1.096	0.658	2.630	3.025	1.505	1.753
1.5_2.25_3	262.57	800.02	0.20	0.345	0.689	1.034	2.585	2.844	1.131	1.724
1.5_2.75_4	277.55	855.08	0.20	0.289	0.770	1.156	2.889	3.443	1.171	1.926
0.5_2.25_4	284.86	882.17	0.20	0.168	1.353	0.676	3.043	4.185	1.678	2.029
1.5_3_3	262.55	799.93	0.20	0.345	0.689	1.034	2.585	3.619	1.130	1.723
1_2.25_3.5	265.04	809.06	0.20	0.251	0.878	0.878	2.634	3.105	1.280	1.756

view, mechanical or optical devices can be used for measuring the principal strain values in the sheet plane, which are equal for both axes (Ox and Oy).

Fig. 17 plots the hardening curves in Table 3 with $r_0=r_{90}$ and the points obtained using the membrane theory (Eq. (10)) under isotropy conditions, as recommended by ISO 16808:2014 [21]. The respective error in equivalent stress is shown in Fig. 18. This error is defined as: Error $=(\bar{\sigma}_{HL}-\bar{\sigma}_{MT})/\bar{\sigma}_{HL}$ (where $\bar{\sigma}_{HL}$ and $\bar{\sigma}_{MT}$ are the equivalent stresses given by the hardening law (*HL*) and the estimated from the membrane theory (*MT*), respectively). The observed errors arise from the determination of the radius of curvature and are also associated to the use of the membrane theory approach under bulge test conditions.

4.3. *In-plane anisotropic materials with $r_0\neq r_{90}$*

The materials with planar anisotropy such that $r_0\neq r_{90}$ (Tables 3 and 4) are now analysed. In these cases, the stress and strain paths are different from 1 (see Figs. 12 and 13 and Table 3) and the simplified equation of the membrane theory (Eq. (10)) does not allow calculating the stresses σ_1 and σ_2, separately. Alternatively, the use of Eq. (9) requires the knowledge of the stress path, in order to obtain the stresses σ_1 and σ_2. Besides, Eq. (9) assumes a linear relationship between σ_2 and σ_1 with slope equal to -1, at each moment of deformation (p and t fixed), assuming that $\rho_1=\rho_2=\rho$ (see Section 3.2), and its interception with the equibiaxial stress line corresponds to the stress determined by using the simplified equation of the membrane theory (Eq. (10)). This is exemplified in Fig. 19 for the initial yield surface of the Hill'48 anisotropic material 0.5_2.25_4, which is crossed by the von Mises surface at the point corresponding to the observed stress path. The figure also shows the von Mises surface corresponding to an equivalent stress equal to the determined using the simplified equation of the membrane theory (Eq. (10)), *i.e.* when considering $\bar{\sigma}=\sigma(=\sigma_1=\sigma_2)$. The equivalent stresses corresponding to both von Mises surfaces can be significantly different, depending on the anisotropy of the material.

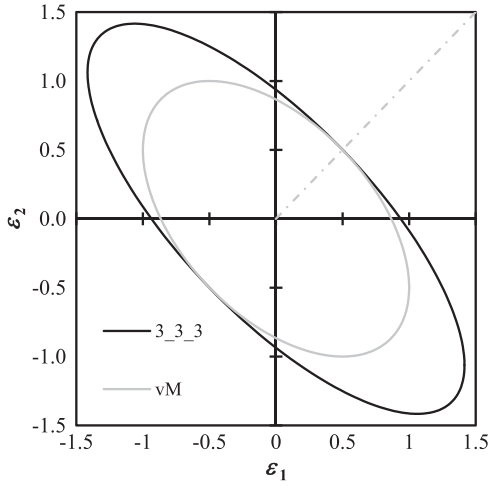

Fig. 16. Curves of equivalent plastic strain equal to 1, for the Hill'48 material 3_3_3 and for the equivalent isotropic von Mises material (see Fig. 15(a)). The dashed-dotted line represents the equibiaxial strain path.

Moreover, the results show that the equivalent strains obtained

Table 4
Constitutive parameters equivalent to those in Table 1 for the materials 200_0.10 and 200_0.35 in Table 2. The average stress paths observed during the bulge test and the k value are also indicated. Only three cases of anisotropy are considered: 0.6_0.7_0.8, 1.5_2.75 and 0.5_2.25_4.

Material	Parameters of the Swift law			Parameters of the Hill'48 criterion						
	Y_0 [MPa]	K [MPa]	n	F	G	H	$L=M$	N	σ_2/σ_1	k
0.6_0.7_0.8	192.91	326.51	0.10	0.436	0.581	0.349	1.396	1.222	1.117	0.930
	192.78	1215.69	0.35	0.436	0.581	0.348	1.394	1.220	1.108	0.929
1.5_2.75_4	277.61	487.28	0.10	0.289	0.771	1.156	2.890	3.345	1.173	1.927
	277.55	1988.43	0.35	0.289	0.770	1.156	2.889	3.443	1.171	1.926
0.5_2.25_4	286.80	505.05	0.10	0.171	1.372	0.685	3.084	4.242	1.712	2.056
	284.97	2060.57	0.35	0.169	1.354	0.676	3.045	4.188	1.680	2.030

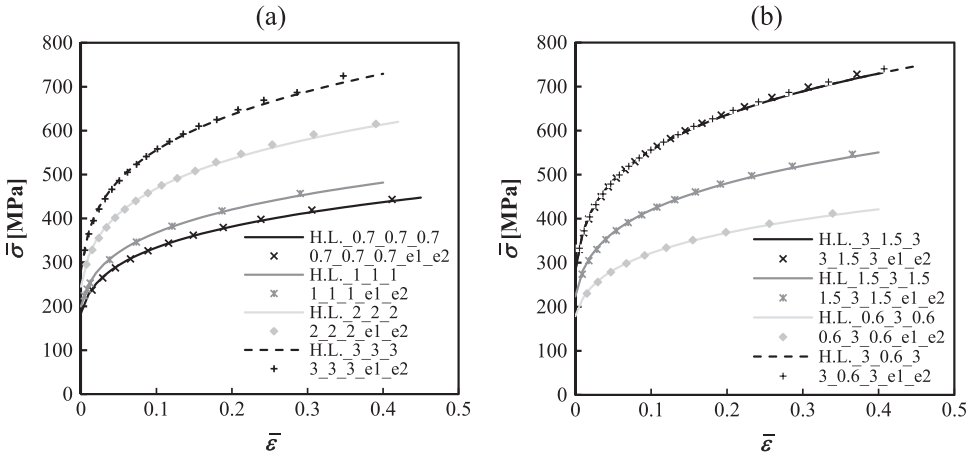

Fig. 17. Comparison between the hardening curves in Table 3 (lines) and the results obtained with the membrane theory (symbols), whatever the criterion used for determining the equivalent stress and strain (von Mises or Hill'48) for: (a) in-plane isotropic materials ($r_0 = r_{45} = r_{90}$); (b) materials with $r_0 = r_{90} \neq r_{45}$. The hardening coefficient of the materials is $n = 0.20$ (Table 3).

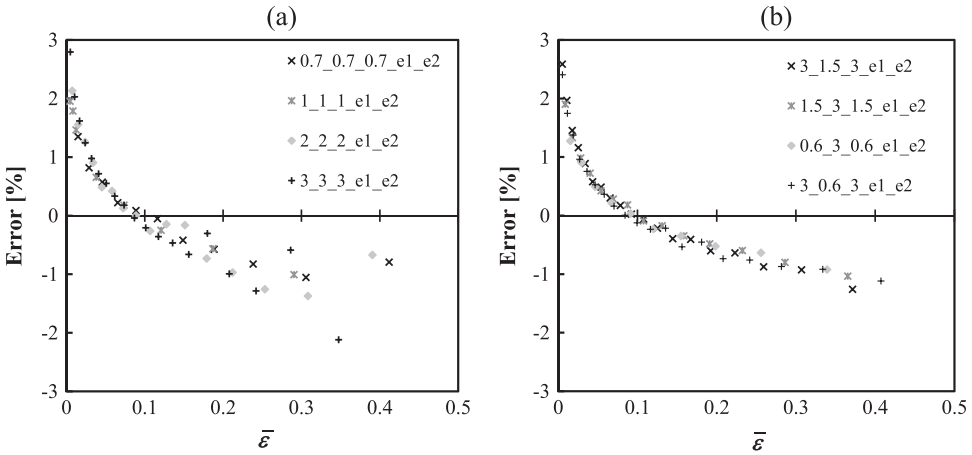

Fig. 18. Evolution of the error in stress for the cases of Fig. 17 for: (a) in-plane isotropic materials ($r_0 = r_{45} = r_{90}$); (b) materials with $r_0 = r_{90} \neq r_{45}$. The hardening coefficient of the materials is $n = 0.20$ (Table 3).

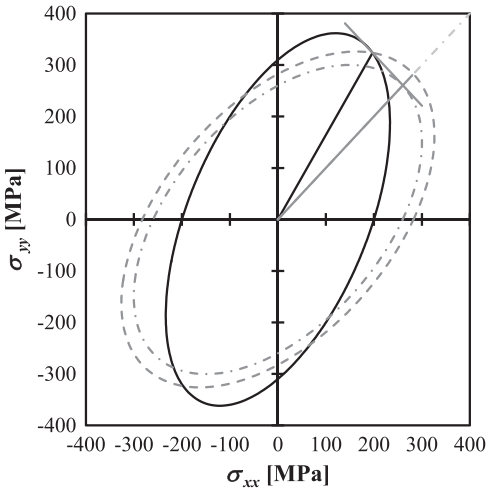

Fig. 19. Initial yield surfaces of the material 0.5_2.25_4 with $n = 0.20$ (black solid line) and two isotropic materials with equivalent stress equal: (i) to that of the anisotropic Hill'48 material (dashed line) and (ii) to the stress determined using the simplified equation of the membrane theory (Eq. (10) – dashed-dotted line). The biaxial stress path observed during the bulge test (black solid line) and the equibiaxial stress path (grey solid line) are also indicated. The line with negative slope corresponds to the equation ($\sigma_2 + \sigma_1 = \text{constant}$, *i.e.* Eq. (9)).

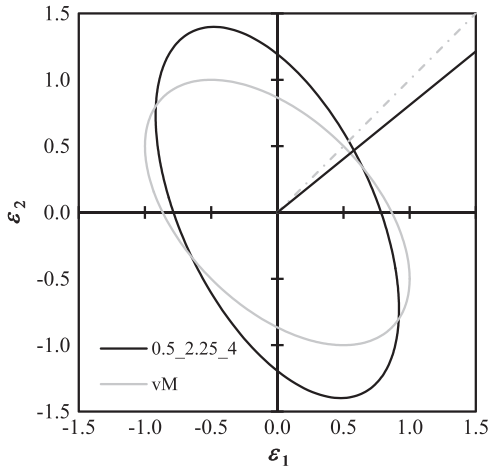

Fig. 20. Curves of equivalent strain equal to 1, for the material 0.5_2.25_4 (black solid line) and the equivalent isotropic material (grey solid line). The observed strain path (solid straight line) is also indicated as well as the equibiaxial strain path (dashed-dotted straight line).

using the Hill'48 or the von Mises yield criterion (Eqs. (22) and (23), respectively) are different for materials with $r_0 \neq r_{90}$. This is illustrated in Fig. 20 for the case of the material 0.5_2.25_4, which shows, in the (ε_1; ε_2) plane, the curves with equal value of equivalent strain ($\bar{\varepsilon} = 1$), for the Hill'48 and the equivalent von Mises criteria. The curves with

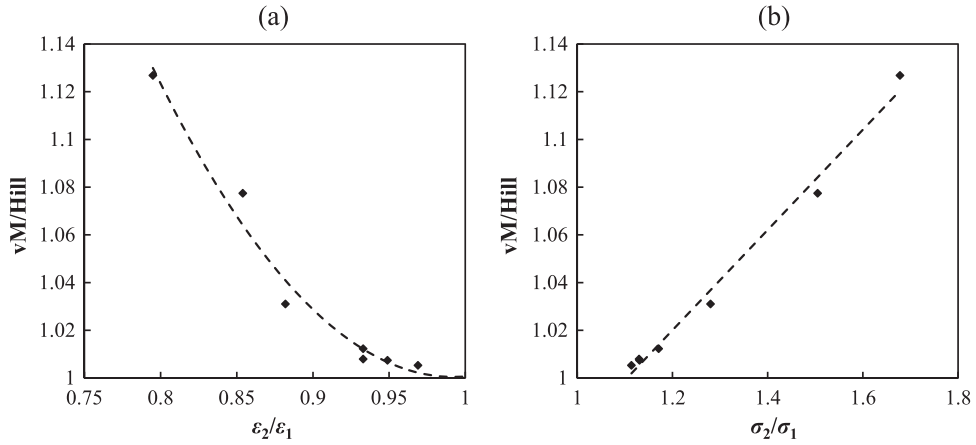

Fig. 21. Ratio between the equivalent strains determined by von Mises and Hill'48 for the materials with $r_0 \neq r_{90}$ and $n = 0.20$ (see Table 3), as a function of: (a) the strain path; (b) the stress path. The dashed lines highlight the trend of the evolutions.

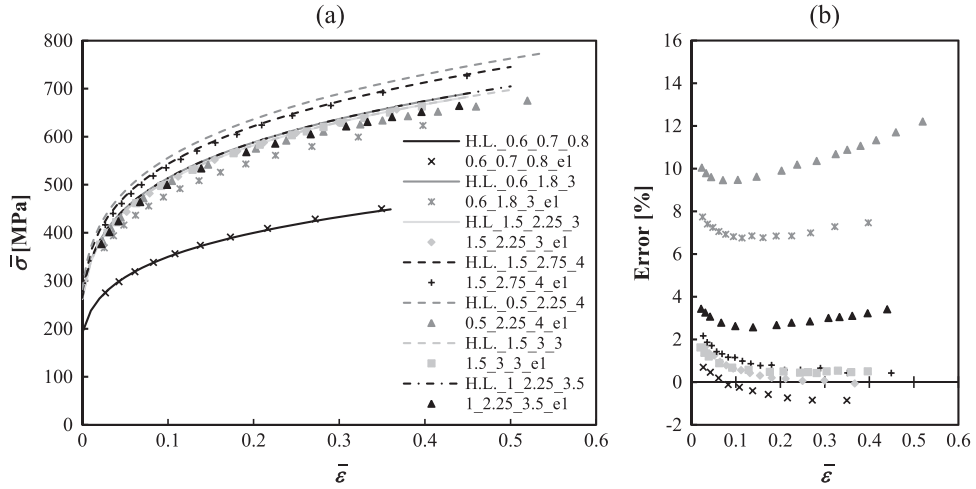

Fig. 22. (a) Comparison between the hardening laws in Table 3 (lines) and the results obtained by the membrane theory (symbols) with $\sigma_1 = \sigma_2 = \sigma = \bar{\sigma}$ (Eq. (18)). The equivalent strain determination uses the value of ε in Eq. (24) equal to the measured value of ε_1; (b) evolution of the error in equivalent stress with the equivalent strain. The hardening coefficient of the materials is $n = 0.20$ (Table 3).

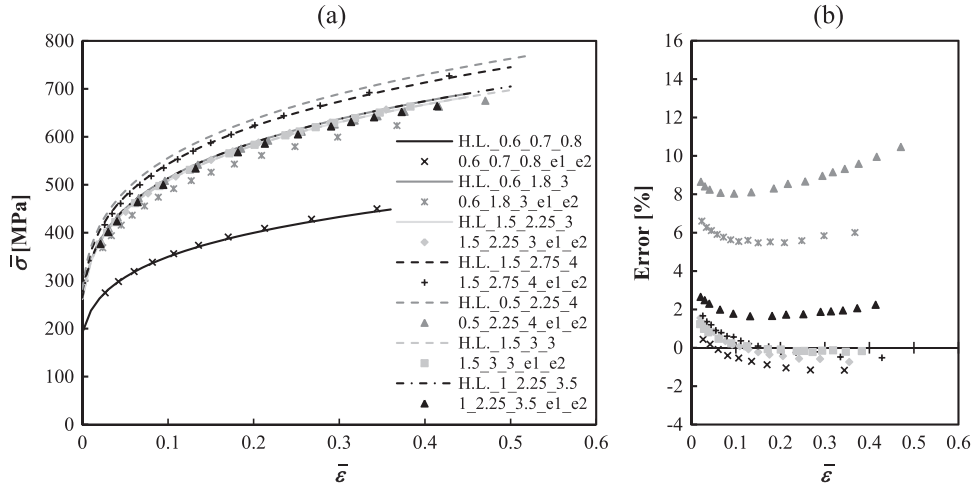

Fig. 23. (a) Comparison between the hardening laws in Table 3 (lines) and the results by the membrane theory (symbols) with $\sigma_1 = \sigma_2 = \sigma = \bar{\sigma}$ (Eq. (18)). The equivalent strain determination uses the measured values of ε_1 and ε_2 in Eq. (23); (b) evolution of the error in equivalent stress with the equivalent strain. The hardening coefficient of the materials is $n = 0.20$ (Table 3).

equal equivalent strain intersect each other at a point other than that corresponding to the observed strain path.

In order to assess the error in the determination of the equivalent strain under the assumption of equibiaxial strain path and von Mises criterion (Eq. (23)), when compared with the value determined by the Hill'48 definition (Eq. (22)), Fig. 21 shows the ratio between the von Mises and the Hill'48 equivalent strains as a function of the strain and stress paths (Fig. 21(a) and (b), respectively), observed for all materials

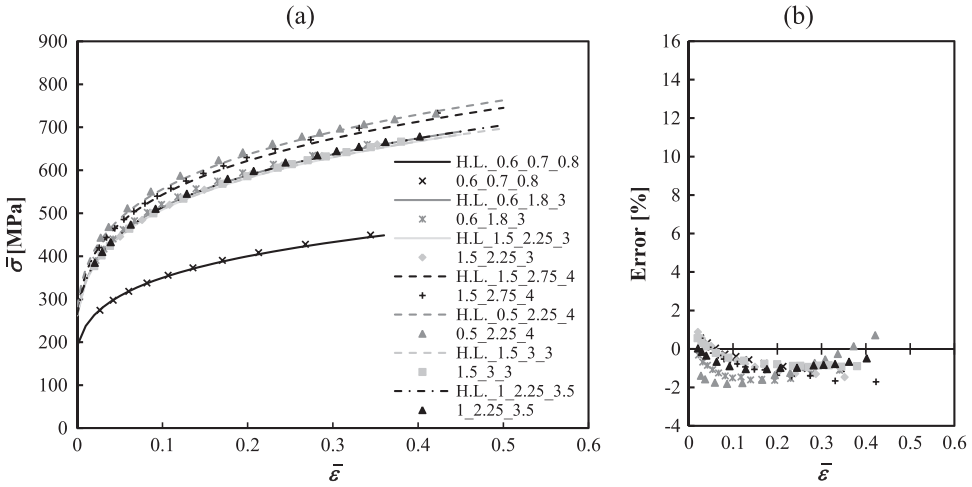

Fig. 24. (a) Comparison between the hardening laws in Table 3 (lines) and the results obtained by the membrane theory (symbols) using the Hill'48 stress and strain definitions; (b) evolution of the error in equivalent stress with the equivalent strain. The hardening coefficient of the materials is $n=0.20$.

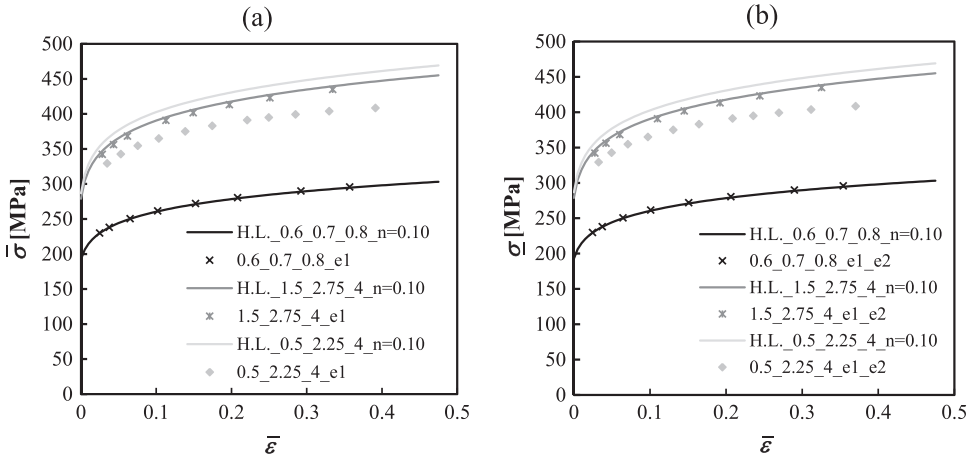

Fig. 25. Comparison between the hardening laws in Table 4 (lines) and the results obtained by the membrane theory (symbols) with $\sigma_1=\sigma_2=\sigma=\bar{\sigma}$ (Eq. (18)). The equivalent strain determination uses the values of: (a) ε in Eq. (24) equal to the measured value of ε_1; (b) the measured values of ε_1 and ε_2 in Eq. (23). The hardening coefficient of the materials is $n=0.10$ (Table 4).

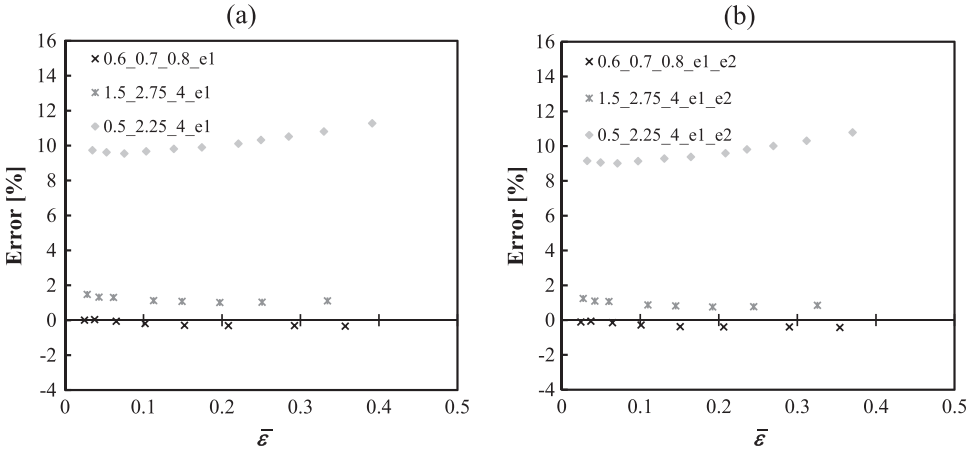

Fig. 26. Evolution of the error in equivalent stress corresponding to: (a) Fig. 25(a); (b) Fig. 25(b).

with $r_0 \neq r_{90}$ and hardening coefficient, $n=0.20$ (Table 3). This ratio follows a quasi-linear relationship with the stress path, but this does not occur with the strain path. When the strain and stress paths are close to 1, both equivalent strains are nearly equal. Differences between von Mises and Hill'48 equivalent strains are clearly noticeable only for the stress paths higher than about 1.1 (or strain paths lower than about 0.95). For the extreme case of the studied materials, 0.5_2.25_4, the ratio between the equivalent strains determined by von Mises and Hill'48 is about 1.13.

In summary, the biaxial stress *vs.* curve determined under the assumption of the simplified membrane theory equation, as recommended by ISO 16808:2014 [21], and resorting to the von Mises definitions of equivalent stress and strain can be significantly inaccurate, in case of materials with $r_0 \neq r_{90}$, as will be seen in the next. Two

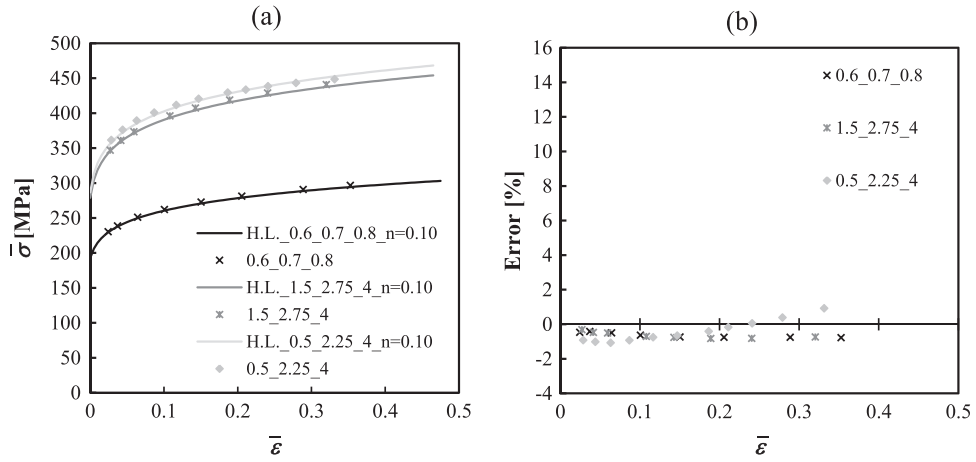

Fig. 27. (a) Comparison between the hardening laws in Table 4 (lines) and the results obtained by the membrane theory (symbols) using the Hill'48 stress and strain definitions; (b) evolution of the errors in equivalent stress with the equivalent strain. The hardening coefficient of the materials is $n=0.10$.

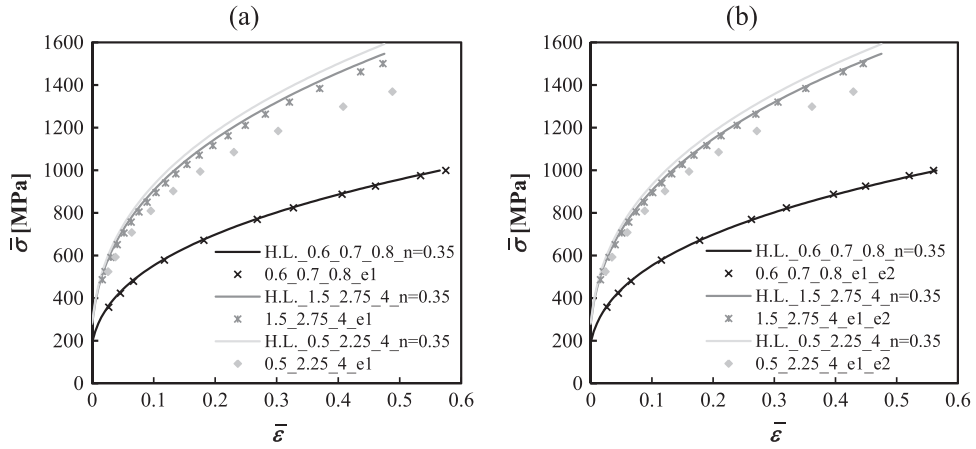

Fig. 28. Comparison between the hardening laws in Table 4 (lines) and the results obtained by the membrane theory (symbols) with $\sigma_1=\sigma_2=\sigma=\bar{\sigma}$ (Eq. (18)). The equivalent strain determination uses: (a) the value of ε in Eq. (24) equal to the measured value of ε_1; (b) the measured values of ε_1 and ε_2 in Eq. (23). The hardening coefficient of the materials is $n=0.35$.

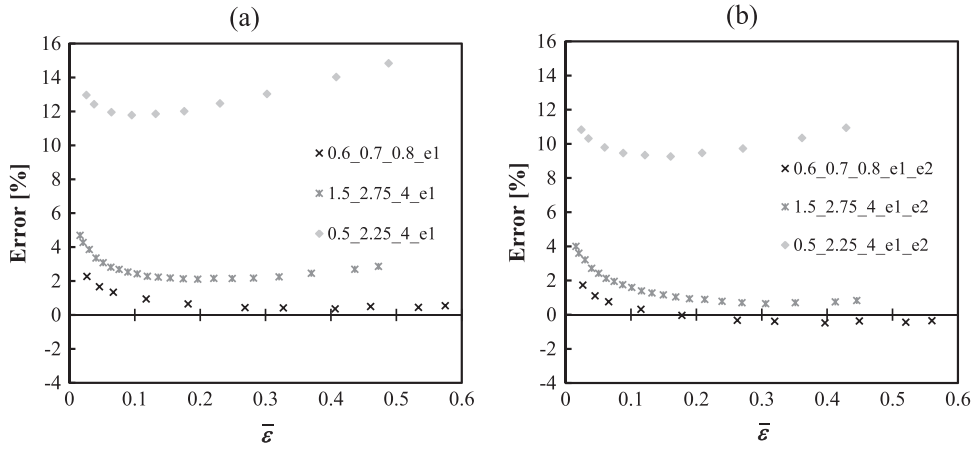

Fig. 29. Evolution of the error in equivalent stress corresponding to: (a) Fig. 28(a); (b) Fig. 28(b).

different approaches commonly used are analysed, according to the strain measurement system available:

i) The measurement of the strains and radii of curvature are performed using mechanical devices (see for example [10,30]), *i.e.* an extensometer and a spherometer, respectively. In this case, only one strain value is measured, generally in the rolling direction, ε_1, and the equivalent strain is assumed: $\bar{\varepsilon}=2\varepsilon_1$. The equivalent stress is calculated from the simplified equation of the membrane theory (Eq. (10)), which considers $\bar{\sigma}=\sigma=\sigma_1=\sigma_2$;

ii) The measurement of strains and curvature radii are performed using an optical device, as recommended by ISO 16808:2014 [21]. In this case, it is possible to assess both principal strains ε_1 and ε_2, in order to calculate the equivalent strain using Eq. (23). The membrane theory is used considering $\sigma=\sigma_1=\sigma_2$ (Eq. (10)), in order to calculate the equivalent stress using Eq. (18). This case becomes quite similar to case (i), unless both principal strains in the sheet plane are known, which allows using Eq. (23) instead of Eq. (24) for

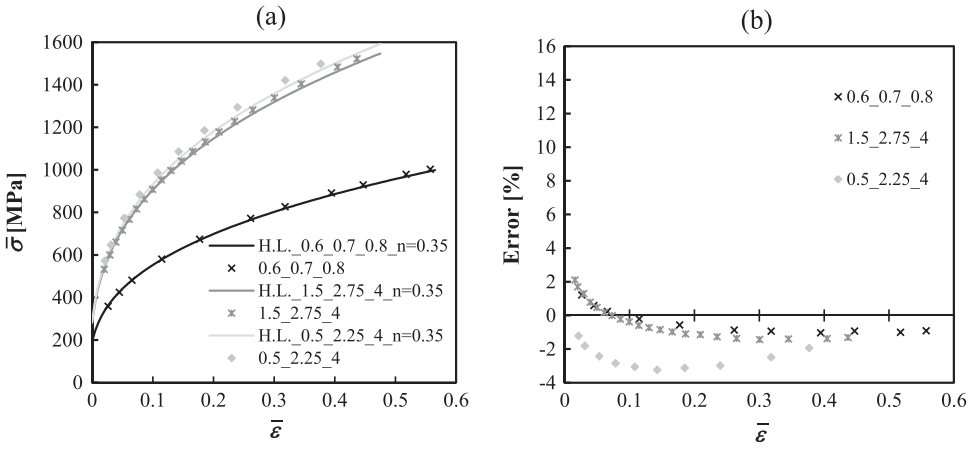

Fig. 30. (a) Comparison between the hardening laws in Table 4 (lines) and the results obtained by the membrane theory (symbols) using the Hill'48 stress and strain definitions; (b) evolution of the errors in equivalent stress with the equivalent strain. The hardening coefficient of the materials is $n=0.35$.

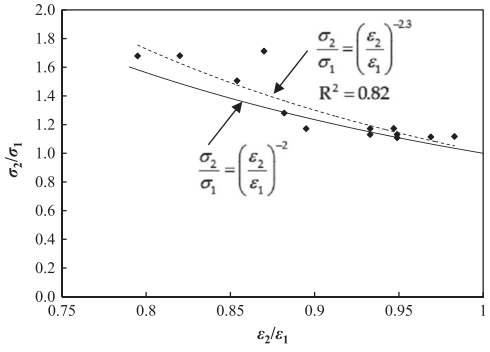

Fig. 31. Stress path *vs.* strain path for Hill'48 materials, with $n=0.10$, 0.20 and 0.35. The fitted curve (dashed line) and respective parameters are also shown. The lower curve (solid line) corresponds to Eq. (25).

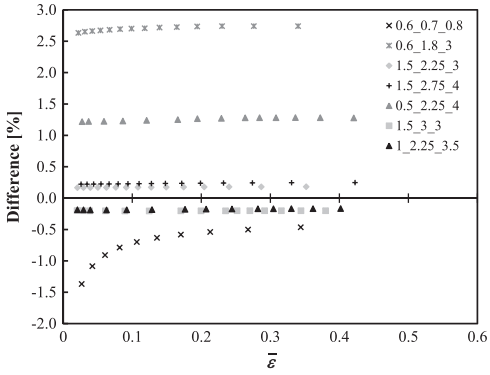

Fig. 33. Difference of error between Figs. 32 and 24, for the materials with $n=0.20$ (Table 3).

determining the equivalent strain; besides, the equivalent stress has the same value as in case (i).

In this context, the biaxial stress *vs.* strain curves of the in-plane anisotropic materials with $r_0 \neq r_{90}$ are now determined using the two previously mentioned approaches. The points of the biaxial stress *vs.* strain curve obtained during the test are compared with the hardening curves in Tables 3 and 4. Figs. 22(a) and 23(a) compares the hardening curves of the materials in Table 3 (with the hardening coefficient $n=0.20$), with the results obtained from the membrane theory (Eq. (10)), considering (as previously mentioned): (i) $\bar{\varepsilon}=2\varepsilon_1$ with the principal strain ε_1 measured along Ox (Fig. 22(a)); (ii) $\bar{\varepsilon}$ determined by the Eq. (23) from the measured values of the principal strains ($\varepsilon_1 \neq \varepsilon_2$) (Fig. 23(b)). Figs. 22(b) and 23(b) show the evolution of the error in equivalent stress with the equivalent plastic strain, corresponding to Figs. 22(a) and 23(a). The errors in equivalent stress are relatively high in both approaches for the materials that show $r_0 < 1$ and $r_{90} > 1$, simultaneously. For the material 0.5_2.25_4, the errors can attain about 12% in Fig. 22(b) and 10% in Fig. 23(b).

It is important to understand the source of the errors shown in

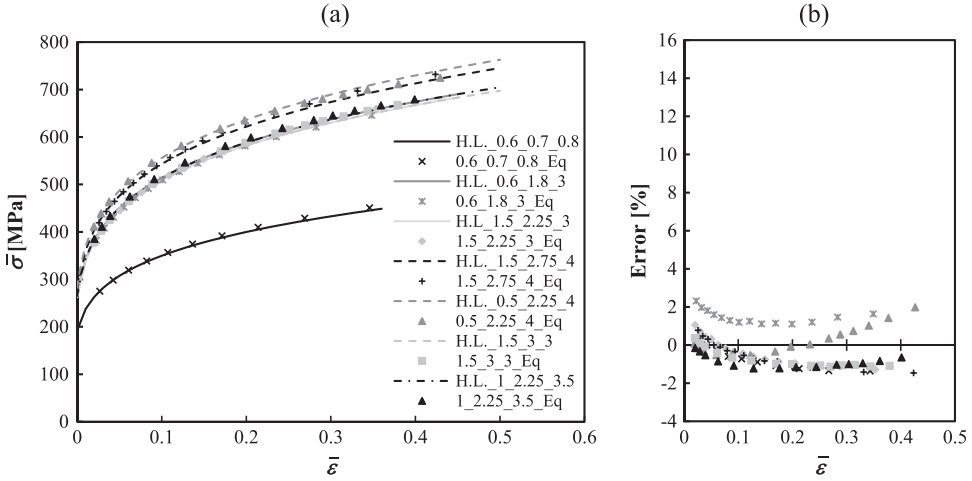

Fig. 32. (a) Comparison between the hardening laws in Table 3 (lines) and the results obtained by membrane theory (symbols) using the Eqs. (25) and (26) for the materials with $n=0.20$; (b) evolution of the corresponding errors in equivalent stress with the equivalent strain.

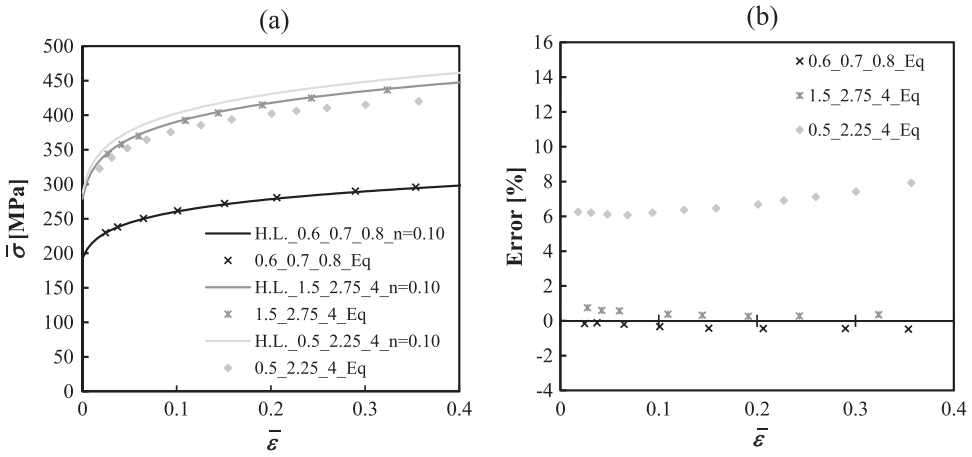

Fig. 34. (a) Comparison between the hardening laws in Table 4 (lines) and the results obtained by membrane theory (symbols) using Eqs. (25) and (26) for the materials with $n=0.10$; (b) evolution of the corresponding errors in equivalent stress with the equivalent strain.

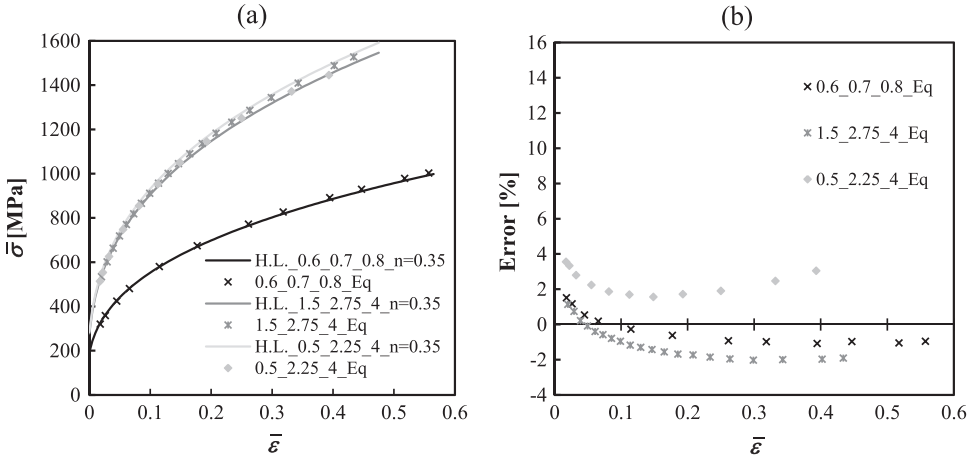

Fig. 35. (a) Comparison between the hardening laws in Table 4 (lines) and the results obtained with membrane theory (symbols) using Eqs. (25) and (26) for the materials with $n=0.35$; (b) evolution of the corresponding errors in equivalent stress with the equivalent strain.

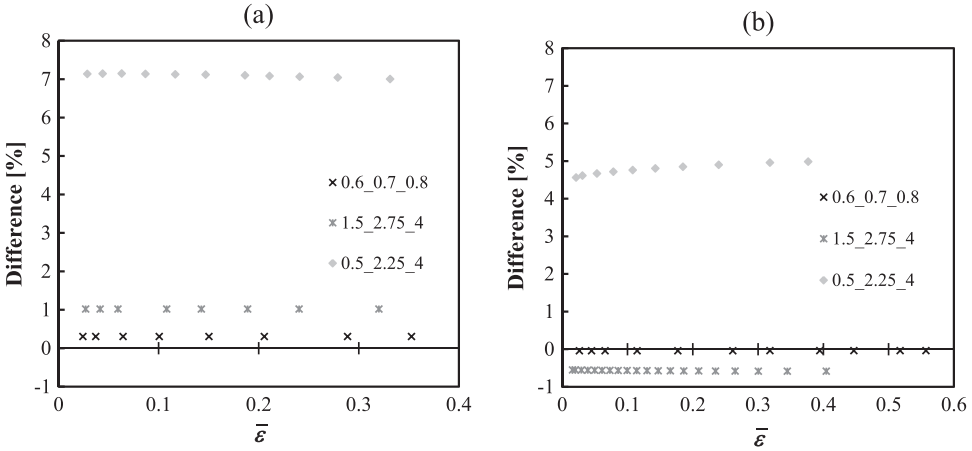

Fig. 36. Difference of error between: (a) Figs. 34(b) and 27(b), for the materials with $n=0.10$ (Table 4); (b) Figs. 35(b) and 30(b), for materials with $n=0.35$ (Table 4).

Figs. 22(b) and 23(b), *i.e.* to what extent the assumptions used in the analysis ($\sigma_1=\sigma_2$ and the von Mises criterion) are behind the errors. In this context, Fig. 24(a) compares the hardening laws in Table 3 with the results obtained taking into account the Hill'48 criterion for determining the stress paths from the observed strain paths (Eqs. (15) or (16)), at the pole of the cap, coupled with the general equation of the membrane theory (Eq. (9)). Fig. 24(b) shows the respective errors in equivalent stress. It should be highlighted that, in general, this is not the experimental case, *i.e.* the anisotropic criterion and respective parameters describing the anisotropy of the material are unknown, which prevents the assessment of the stress path from the strain path (Eqs. (15) or (16)).

For materials with $r_0 \neq r_{90}$, the errors in stress in Fig. 24(b) arise from the determination of the curvature radius and the use of the membrane theory approach under bulge test conditions. Thus, it is appropriate to state that the differences of error in stress between

Table 5
Designation of the materials and the respective parameters of Drucker+L criterion and Voce law. The average stress and strain paths observed during the bulge test are also shown.

Designation	Parameters of the Drucker+L criterion						Parameters of the Voce law			Stress and strain paths	
	C_1	C_2	C_3	$C_4=C_5$	C_6	c	Y_{sat} [MPa]	R_{sat} [MPa]	C_Y	σ_2/σ_1	$\varepsilon_2/\varepsilon_1$
A_c=2	0.684	1.168	1.168	1.168	1.268	2	671.54	356.04	7.16	1.214	0.952
B_c=1	0.669	1.141	1.141	1.141	1.239	1	674.28	357.50	7.19	1.235	0.911
C_c=2	0.750	1.547	1.149	1.281	1.450	2	657.47	348.59	7.01	1.367	0.908
D_c=1	0.676	1.394	1.035	1.219	1.307	1	666.07	353.15	7.10	1.413	0.882
E_c=−1	0.657	1.122	1.122	1.122	1.218	−1	686.26	363.85	7.32	1.319	0.854
F_c=−2	0.658	1.123	1.123	1.123	1.220	−2	696.06	369.05	7.42	1.376	0.832
G_c=−1	0.679	1.400	1.040	1.225	1.313	−1	690.92	366.32	7.36	1.566	0.806
H_c=−2	0.737	1.518	1.127	1.383	1.423	−2	709.73	376.30	7.565	1.665	0.773

Figs. 24(b) and 23(b) (or Fig. 22(a)) are due to the assumptions used for determining the equivalent stress and strain. In this context, it can be concluded that the errors due to the assumptions used in Figs. 22 and 23 are not negligible, particularly in the case of materials 0.5_2.25_4 and 0.6_1.8_3 and even for the material 1_2.25_3.5. These materials have the major axis of the Hill'48 ellipse in the (σ_{xx}; σ_{yy}) plane relatively far away from 45° (see Fig. 4).

Figs. 25–30 show the same kind of results, as for materials with hardening coefficient $n=0.20$ (Figs. 22–24), but for the three anisotropic materials studied with $n=0.10$ and 0.35 (see Table 4). The errors in stress follow the same trend although showing slight differences from those of materials with $n=0.20$. Also, the comparison of the results obtained with von Mises criterion with those from Hill'48 criterion leads to similar conclusions that for materials with $n=0.20$.

In summary, the commonly used experimental approaches to determine the biaxial stress *vs.* strain curve from the bulge test, under the assumption of equibiaxial stress (and also often equibiaxial strain), can lead to relatively high errors, for instance in case of in-plane anisotropic materials with $r_0 \neq r_{90}$ when the axis of the Hill'48 ellipse in the (σ_{xx}; σ_{yy}) plane is relatively far away from 45°.

5. Is it possible to improve the determination of the biaxial stress – strain curve?

To answer the question in the title of this section, the in-plane anisotropic Hill'48 materials studied in the previous sections are firstly analysed, in order to establish a possible methodology. Then, this methodology is tested by means of results using the more flexible Drucker+L and CB2001 yield criteria.

5.1. Methodology development

Fig. 31 plots the stress path *vs.* strain path of these materials, from the average values of the results previously shown in Figs. 12 and 13. Fig. 31 shows that it is possible to fit a power law (dashed line) to establish a correlation between the observed stress and strain paths, which allows a relatively accurate determination of the stress path from the strain path (the point further away from the trend line corresponds to the material 0.5_2.25_4 with $n=0.10$). Fig. 31 also shows a power law (solid line) with exponent equal to −2:

$$\frac{\sigma_2}{\sigma_1} = \left(\frac{\varepsilon_2}{\varepsilon_1}\right)^{-2}. \tag{25}$$

Both equations can be used with good enough accuracy for determining the stress path from the experimentally measured strain path (if using an optical measurement system as recommended by ISO 16808 (2014) [21]), as an alternative to the associated flow rule that needs the *a priori* knowledge of the anisotropic yield criterion and the respective parameters of the material. Eq. (25), with exponent equal to −2, is chosen (instead of the exponent equal to −2.30, which corresponds to the fitted power law) for determining the stress path from the measured strain path. In fact, Eq. (25) ensures that all points in Fig. 31 are very close or above the line defined by this equation, which is not the case of the fitted equation with exponent equal to −2.30. Therefore, Eq. (25) safeguards excesses in determining the stress path, *i.e.* seeks that the evaluated biaxial stress *vs.* strain curve is between those determined, as in Figs. 24(a), 27(a) and 30(a), by one side, and as in Figs. 23(a), 25(b) and 28(b), by other side. Moreover, it safeguards cases of materials with anisotropic behaviour described by other criteria than Hill'48, for which the fitted power law (with exponent equal to −2) may eventually also overestimate the stress path.

In summary, it turns out that in experimental cases of the bulge test, the yield criterion and respective parameters of the material under study are not known. But it is possible to assess the principal strains in the sheet plane by using an optical measurement system and, consequently, the stress path at the pole by using Eq. (25).

Now, the use of Eq. (25) to improve the determination of the stress *vs.* strain curve, presuming that the strain path is measured by digital correlation image technique [21], is analysed. Since the estimated stress path is determined from Eq. (25), it is possible to determine σ_1 and σ_2, using Eq. (9), and then the equivalent stress can be calculated using Eq. (18). The remaining issue is to determine the equivalent strain. This is generally performed using the von Mises criterion. However, as can be seen by comparing, for example, the strain gap between the corresponding points in Figs. 23(b) and 24(b), the value of equivalent strain depends on the yield criteria (see also Figs. 20 and 21). In this context, there exists a simple way to determine the equivalent strain regardless of the yield criterion. In fact, it can be shown that for linear stress and strain paths, which is approximately the case for the bulge test (see Figs. 12 and 13), the definition of plastic work leads to the following relationship:

$$\sigma_1\varepsilon_1 + \sigma_2\varepsilon_2 = \bar{\sigma}\bar{\varepsilon}. \tag{26}$$

The difference in the equivalent strain obtained by using Eq. (26) when compared with Eq. (22) for the Hill'48 materials of Tables 3 and 4 is negligible (less than 0.3%), which indicates that the slight change of the strain path observed during the test does not significantly affects this calculation.

Fig. 32(a) shows the hardening curves of materials in Table 3 with $r_0 \neq r_{90}$ and $n=0.20$, and the obtained points using the suggested strategy, *i.e.* combining the membrane theory (Eq. (9)) with Eqs. (25) and (26). The respective errors in stress are shown in Fig. 32(b). These errors are less than those in Figs. 22 and 23, and quite similar to those in Fig. 24, in which they arise almost entirely from the radius of curvature determination and the use of the membrane theory approach under bulge test conditions.

In order to better quantify the error in equivalent stress due to the procedure now proposed, *i.e.* isolate this error from other sources, the difference in equivalent stress error between those in the Fig. 32(b) and in the Fig. 24(b) are shown in the Fig. 33. This difference of error, lower than 3%, for the material 0.6_1.8_3, lower than 1.5% for 0.6_0.7_0.8 and 0.5_2.25_4, and lower than 0.5%, for all the other materials, shows the capability of the proposed methodology for determining the hardening

Table 6
Designation of the materials and the respective parameters of CB2001 criterion and Voce law. The average stress and strain paths observed during the bulge test are also indicated; "A1" and "A2" represent the first and second order 'anomalous' behaviour [34], respectively.

Designation	Parameters of the CB2001 criterion													Parameters of the Voce law			Stress and strain paths		'Anomalous' behaviour	
	a_1	a_2	a_3	a_4	$a_5=a_6$	c	b_1	b_2	b_3	b_4	b_5	$b_6=b_7=b_8=b_9=b_{11}$	b_{10}	Y_{sat} [MPa]	R_{sat} [MPa]	C_Y	σ_2/σ_1	$\varepsilon_2/\varepsilon_1$	A1	A2
A	1.224	1.120	1.133	1.240	1.170	1.621	1.485	1.415	1.478	1.298	1.116	1.266	1.344	523.86	277.75	5.58	1.000	0.997		✓
B	1.068	1.088	1.115	1.126	1.097	1.808	1.162	1.173	1.258	1.176	1.046	1.148	0.972	507.47	269.06	5.41	1.002	0.995	✓	
C	2.581	1.066	0.853	2.594	0.587	−2.850	−0.578	3.558	0.671	2.110	1.035	0.449	2.400	691.75	366.76	7.37	1.053	0.995		✓
D	1.429	1.945	1.131	1.798	1.052	0.857	5.783	−0.673	−4.735	−3.944	−6.527	1.079	−0.952	533.95	283.10	5.69	1.043	0.968	✓	✓
E	0.558	1.243	0.691	0.630	0.737	1.222	0.630	0.950	0.327	0.469	0.381	0.633	0.142	365.59	193.83	3.90	1.230	0.968		
F	1.848	1.717	2.623	1.283	1.793	1.593	−6.619	5.378	3.691	4.955	2.634	2.401	0.065	766.23	406.25	8.17	1.107	0.962	✓	✓
G	1.167	0.865	1.334	1.212	1.122	0.240	8.264	−0.451	3.986	−3.463	−3.354	1.189	1.694	543.64	288.23	5.79	1.030	0.952	✓	
H	2.999	−1.015	0.561	3.387	3.223	−0.076	−21.280	−41.892	−26.359	−2.319	−48.917	5.787	−52.085	822.39	436.03	8.77	1.147	0.952	✓	✓
I	1.275	−1.751	3.001	2.108	3.031	−0.085	19.960	−11.679	−5.265	−18.067	−43.182	5.276	−7.698	753.06	399.27	8.03	1.301	0.951		
J	1.340	−0.786	2.358	1.142	1.942	−0.03	0.179	−24.343	−21.838	−9.395	−24.348	2.705	−24.348	709.35	376.09	7.56	1.197	0.937	✓	
K	1.457	−0.500	2.183	1.363	2.281	−0.039	9.273	34.903	20.531	4.775	37.253	3.445	37.895	738.15	391.36	7.87	1.284	0.927	✓	✓
L	0.959	0.793	2.077	1.094	1.530	0.303	0.633	−1.008	−0.122	4.381	3.236	1.893	2.120	632.21	335.19	6.74	1.268	0.916		
M	1.479	1.236	1.830	1.328	1.130	2.142	1.057	0.478	1.206	−2.913	−0.996	1.202	−0.325	655.43	347.51	6.99	1.162	0.901	✓	✓
N	1.233	0.417	2.370	1.516	2.426	0.009	−20.248	15.705	−10.107	−2.079	−34.016	3.780	23.014	688.57	365.08	7.34	1.385	0.894		
O	1.591	0.394	2.069	2.258	2.848	−0.083	−0.055	−23.584	−2.844	−11.529	−43.262	4.807	0.236	723.50	383.60	7.71	1.397	0.885		
P	0.339	3.048	3.545	1.640	2.269	1.091	3.716	−11.184	−10.237	−0.052	−4.275	3.418	−3.634	672.69	356.66	7.17	1.542	0.862		
Q	1.160	1.375	1.578	1.368	1.347	1.784	−0.723	−1.096	1.464	−1.700	−1.075	1.563	−0.748	591.61	313.67	6.31	1.204	0.860	✓	
R	0.849	1.663	2.375	1.577	2.131	0.029	−11.034	29.205	30.803	5.615	−0.946	3.110	16.547	642.02	340.40	6.84	1.666	0.808		
S	1.753	0.631	2.126	1.520	1.943	0.142	3.510	10.921	−3.724	2.729	3.937	2.708	7.834	695.58	368.79	7.41	1.458	0.774		

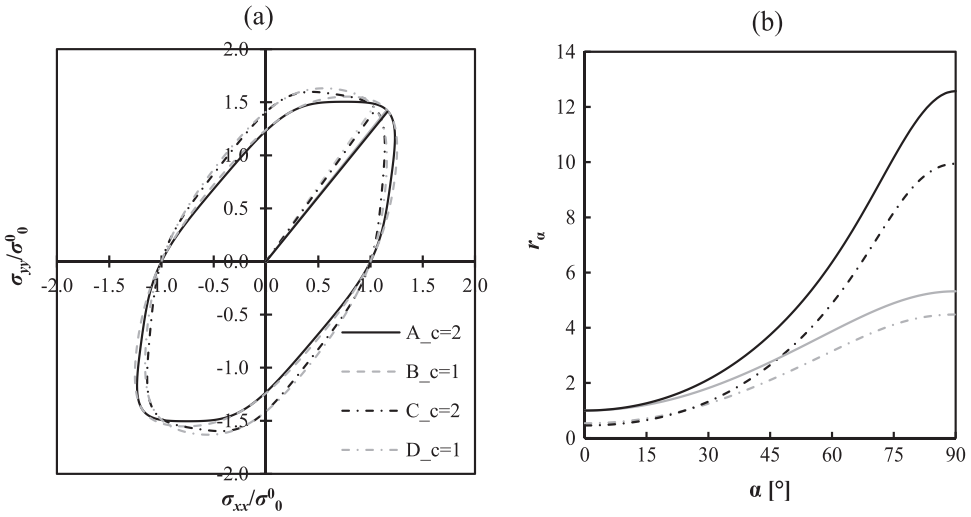

Fig. 37. Drucker+L materials in Table 5, with $c > 0$: (a) normalized initial yield surfaces in the plane (σ_{xx}/σ^0_0; σ_{yy}/σ^0_0) and corresponding stress paths; (b) distribution of r_α in the sheet plane.

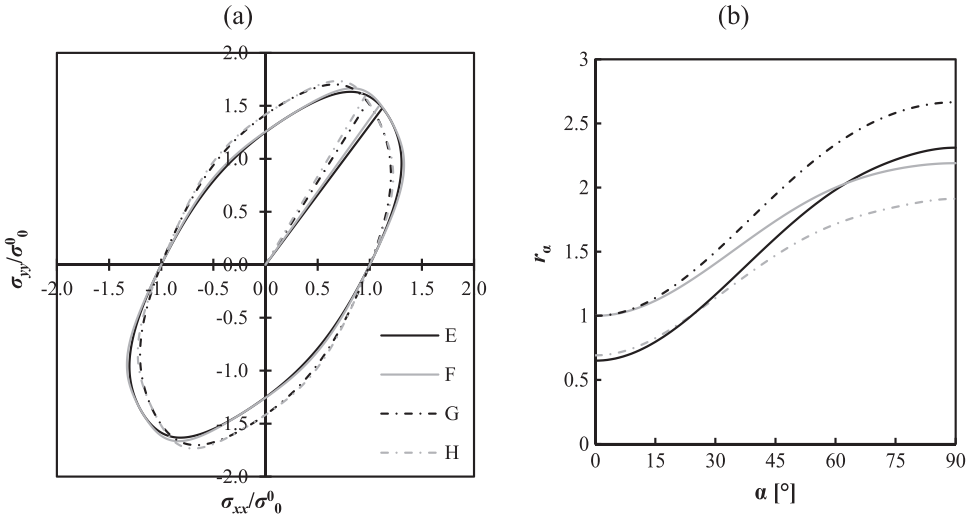

Fig. 38. Drucker+L materials in Table 5, with $c < 0$: (a) normalized initial yield surfaces in the plane (σ_{xx}/σ^0_0; σ_{yy}/σ^0_0) and corresponding stress paths; (b) distribution of r_α in the sheet plane.

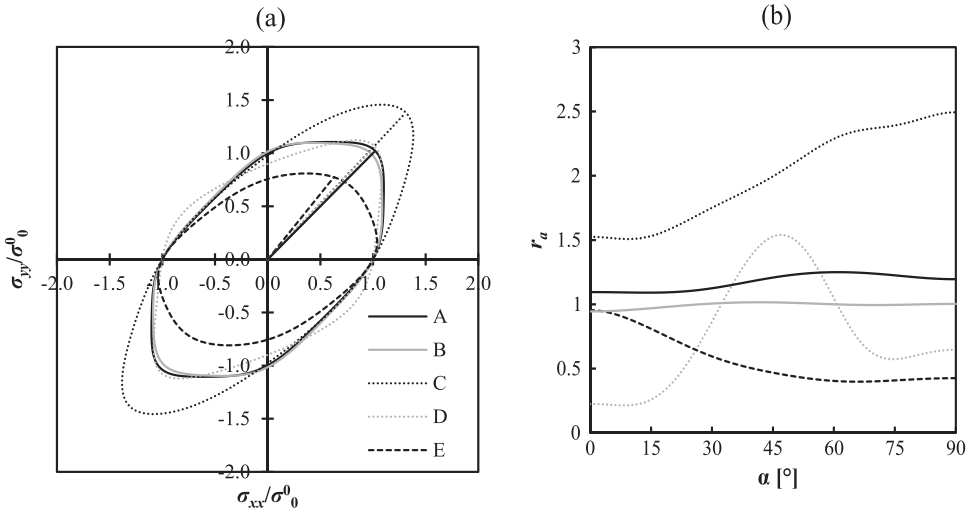

Fig. 39. CB2001 materials "A" to "E" in Table 6: (a) normalized initial yield surfaces in the plane (σ_{xx}/σ^0_0; σ_{yy}/σ^0_0) and corresponding stress paths; (b) distribution of r_α in the sheet plane.

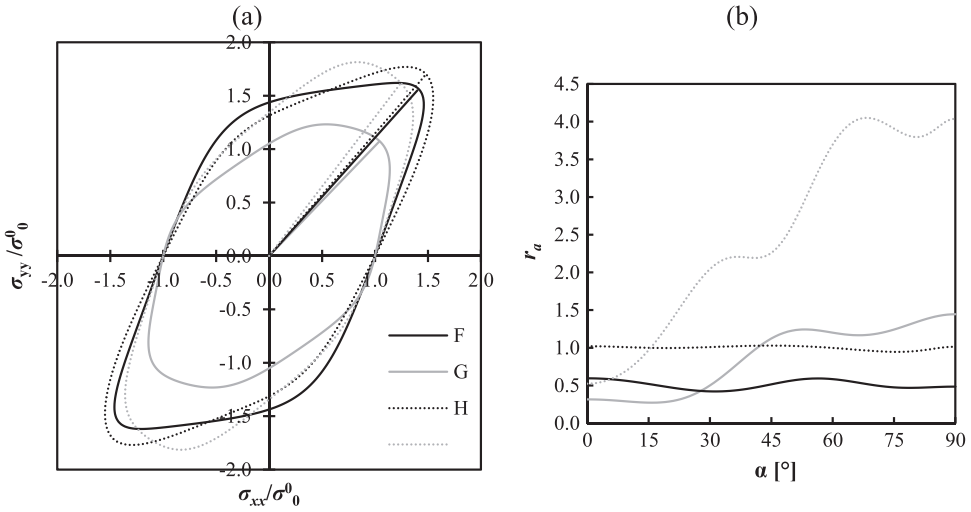

Fig. 40. CB2001 materials "F" to "I" in Table 6: (a) normalized initial yield surfaces in the plane (σ_{xx}/σ^0_0; σ_{yy}/σ^0_0) and corresponding stress paths; (b) distribution of r_α in the sheet plane.

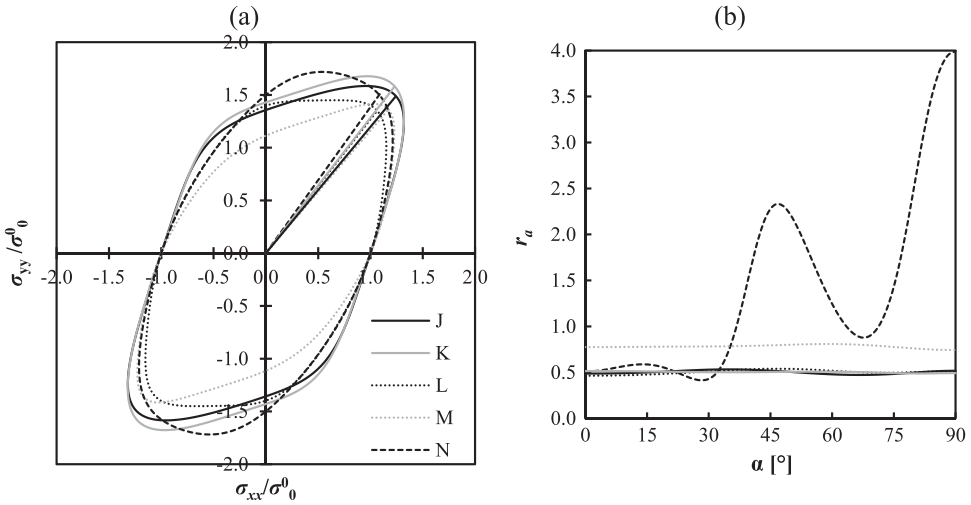

Fig. 41. CB2001 materials "J" to "N" in Table 6: (a) normalized initial yield surfaces in the plane (σ_{xx}/σ^0_0; σ_{yy}/σ^0_0) and corresponding stress paths; (b) distribution of r_α in the sheet plane.

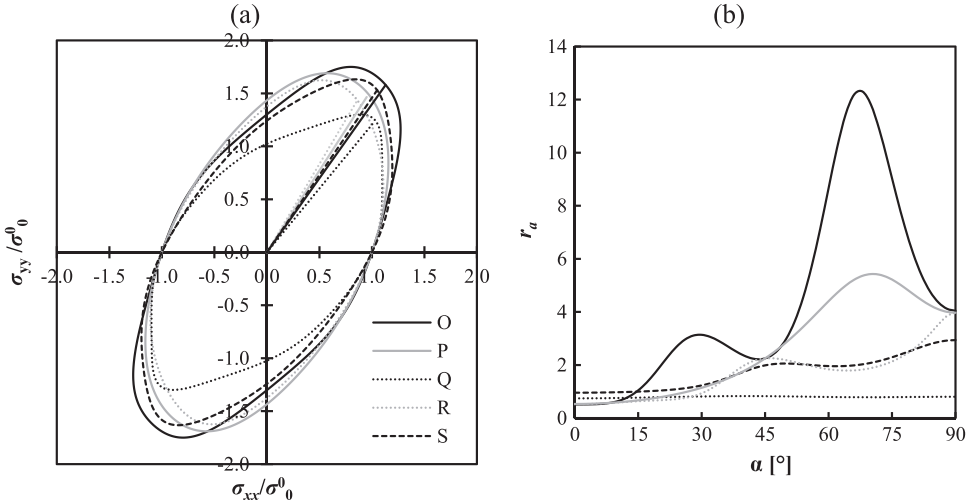

Fig. 42. CB2001 materials "O" to "S" in Table 6: (a) normalized initial yield surfaces in the plane (σ_{xx}/σ^0_0; σ_{yy}/σ^0_0) and corresponding stress paths; (b) distribution of r_α in the sheet plane.

curve.

Similarly to Fig. 32(a), the Figs. 34(a) and 35(a) show the hardening curves of the materials with $n=0.10$ and 0.35 (Table 4), having $r_0 \neq r_{90}$ and the obtained points using the suggested strategy, combining the membrane theory (Eq. (9)) with Eqs. (25) and (26). The respective errors in equivalent stress are shown in Figs. 34(b) and 35(b). For the case of the material 0.5_2.25_4, the level of error is still relatively high, but lower than that obtained using the procedure proposed by ISO

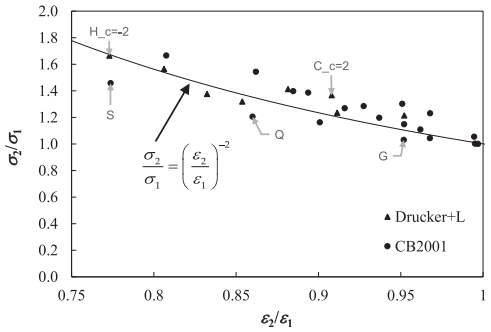

Fig. 43. Stress *vs.* strain path for Drucker + L (triangles) and CB2001 (circles) materials. The curve (solid line) corresponds to Eq. (25). The labelled points correspond to those materials whose analysis is shown in the following figures.

standard (Fig. 29(b)). The difference in equivalent stress error between those in Figs. 34(b) and 35(b), and those in Figs. 27(b) and 30(b), respectively, are shown in Fig. 36 (Fig. 36(a) is identical to Fig. 33 but for n values equal to 0.10; and Fig. 36(b) is identical to Fig. 33 but for n values equal to 0.35).

5.2. Testing the methodology for more flexible yield criteria

Materials with anisotropic behaviour described by non-quadratic yield criteria, namely the Drucker + L (Eq. (2)) and the CB2001 criterion (Eq. (5)) are now analysed, in order to test the reliability of the methodology. Examples of materials described by yield surfaces with different shapes at the region around the equibiaxial stress path are selected, particularly flattened and sharp surfaces. Some of the CB2001 materials exhibit the "first and/or second order anomalous" behaviours [34], and so significantly different from Hill'48 yield surfaces. The Voce law (Eq. (8)) is now chosen for describing the hardening behaviour of the materials.

5.2.1. Cases under analysis

The constitutive parameters of the analysed materials are given in Table 5 (Drucker + L criterion and Voce law) and Table 6 (CB2001 criterion and Voce law). The designation adopted for each material corresponds to a capital letter, followed by the value of the isotropic parameter c, in case Drucker + L materials. In each table the materials are organized according to the value of the strain path observed at the pole of the cap, from the highest to the smallest; these tables also show the observed stress paths. The hardening parameters in Tables 5 and 6 refer to curves corresponding to the observed stress paths. Figs. 37 and 38(a) display the Drucker + L yield surfaces in the plane ($\sigma_{xx}/\sigma^0{}_0$; $\sigma_{yy}/\sigma^0{}_0$). Figs. 37 and 38(b) shows the respective evolutions of the anisotropy coefficient, r_α, in the sheet plane. Figs. 39–42(a) display the CB2001 yield surfaces in the plane ($\sigma_{xx}/\sigma^0{}_0$; $\sigma_{yy}/\sigma^0{}_0$). Figs. 39–42(b) show the respective evolutions of the anisotropy coefficient, r_α, in the sheet plane.

5.2.2. Results and analysis

Fig. 43 shows the observed stress path *vs.* strain path of the Drucker + L and CB2001 materials (see Tables 5 and 6). The curve representing Eq. (25) is also shown. As for Fig. 31, most points in Fig. 43 are close or above the line defined by this equation. Two points below this line, corresponding to the CB2001 materials "Q" and "S" in Table 6 are at some distance from it. This means that, for these two materials, the use of Eq. (25) visibly overestimates the stress path. The consequence of the results of Fig. 43 in determining the biaxial stress *vs.* strain curves is now analysed using illustrative examples concerning: (i) two Drucker + L materials, "C_c = 2" and "H_c = − 2" in Table 5, placed on and above the line defined by Eq. (25); and (ii) three CB2001 materials, "G", "Q" and "S" in Table 6, all below the line defined by Eq. (25) (see Fig. 43).

Fig. 44(a) shows the hardening curves of two materials with anisotropic behaviour described by the Drucker + L criterion ("C_c = 2" and "H_c = − 2", in Table 5) and the points obtained by the suggested strategy. The respective errors in equivalent stress are shown in Fig. 44(b). Fig. 45 shows the results of the biaxial stress *vs.* strain curves of the same two Drucker + L materials ("C_c = 2" and "H_c = − 2", in Table 5), obtained using the membrane theory (Eq. (10)) and $\bar{\varepsilon}$ determined by Eq. (23), based on the measured values of the principal strains ($\varepsilon_1 \neq \varepsilon_2$), as recommended by ISO 16808:2014. As for the Hill'48 materials, a high level of error that can attain 10%, is obtained when the strain path is away from 1 (material H_c = -2–$\varepsilon_2/\varepsilon_1 = 0.773$). The error is relatively low for the other illustrative example (material C_c = 2–$\varepsilon_2/\varepsilon_1 = 0.908$), but it still attains about 3%. Fig. 46 shows the results obtained with the membrane theory (Eq. (9)), taking into account the observed stress and strain paths; the equivalent stress was determined using the Drucker + L definition and the equivalent strain using Eq. (26). The errors of the suggested strategy (Fig. 44(b)) are quite similar to those in Fig. 46(b) and smaller than 2%, for both cases. The analysis of the other Drucker + L materials, in Table 5, leads to the same conclusion: the errors arising from the use of the proposed methodology are insignificant.

Figs. 47–49 show the same type of results as the last three figures, but for three materials ("G", "Q" and "S", in Table 6) with anisotropic behaviour described by the CB2001 criterion. These three cases were chosen as illustrative examples because their stress and strain paths put them below the line defined by Eq. (25) and, therefore, the use of this equation overestimates the stress path (see Fig. 43). In case of the material "G" the error is quite low, whatever the methodology for determining the stress *vs.* strain curve (Figs. 47–49). For the other two

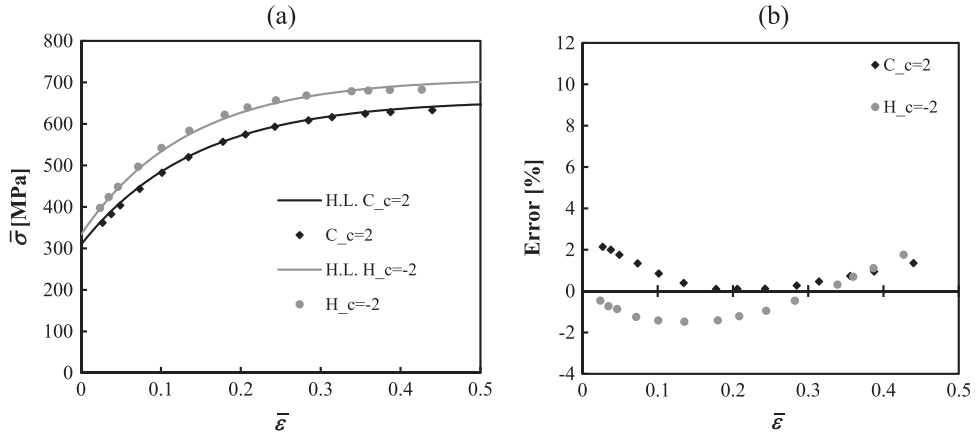

Fig. 44. (a) Comparison between the hardening laws of Drucker + L materials "C_c = 2" and "H_c = − 2" in Table 5 (lines) and the results obtained by the membrane theory (symbols) using the Eqs. (25) and (26); (b) evolution of the corresponding errors in equivalent stress with the equivalent strain (see Fig. 43).

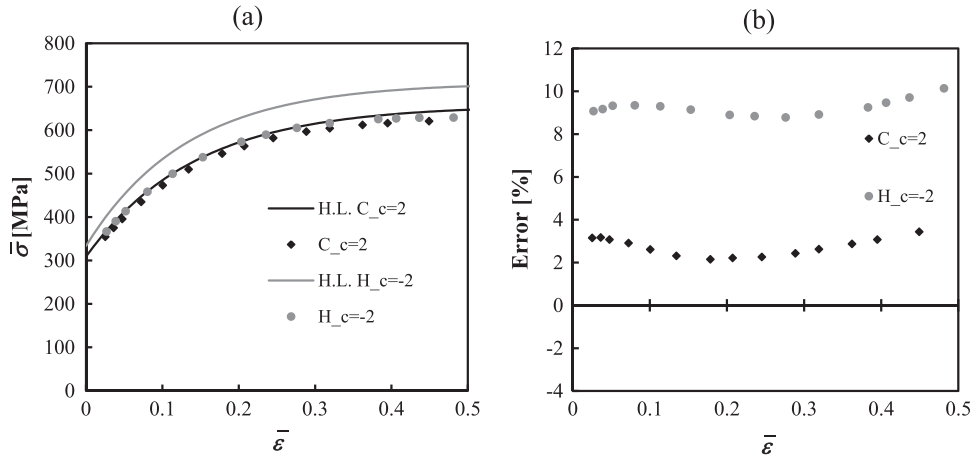

Fig. 45. (a) Comparison between the hardening laws of Drucker + L materials "C_c = 2" and "H_c = − 2" in Table 5 (lines) and the results obtained by the membrane theory (symbols) with $\sigma_1 = \sigma_2 = \sigma = \bar{\sigma}$ (Eq. (18)). The equivalent strain determination uses the measured values of ε_1 and ε_2 in Eq. (23); (b) evolution of the error in equivalent stress with the equivalent strain (see Fig. 43).

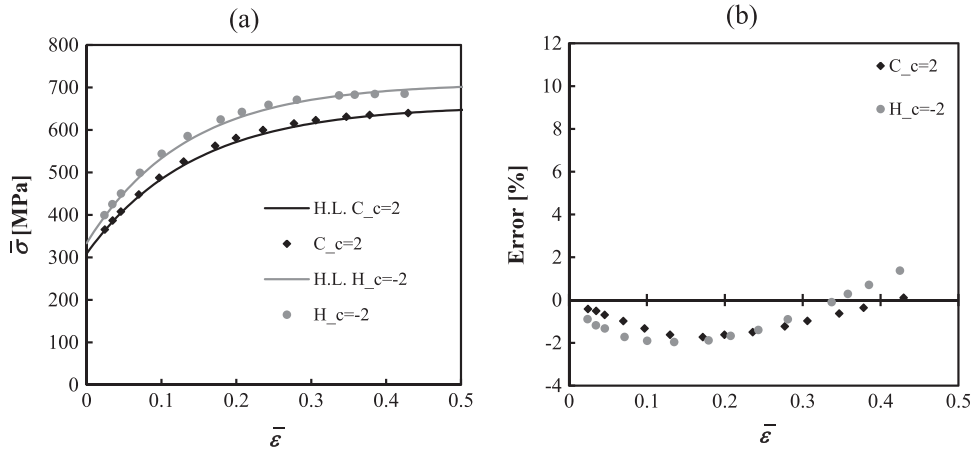

Fig. 46. (a) Comparison between the hardening laws of Drucker + L materials "C_c = 2" and "H_c = − 2" in Table 5 (lines) and the results obtained with membrane theory (symbols) using the Drucker + L equivalent stress definition and Eq. (26); (b) evolution of the error in equivalent stress with the equivalent strain.

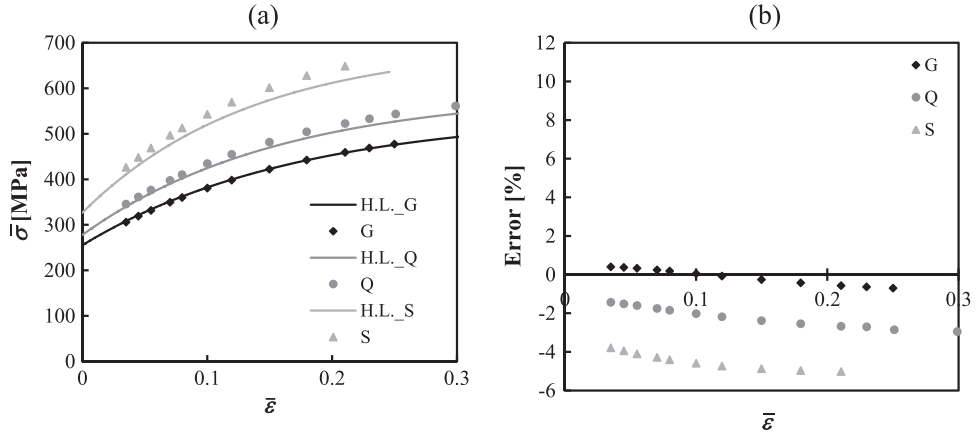

Fig. 47. (a) Comparison between the hardening laws of CB2001 materials "G", "Q" and "S" in Table 6 (lines) and the results obtained by the membrane theory (symbols) using the Eqs. (25) and (26); (b) evolution of the corresponding errors in equivalent stress with the equivalent strain (see Fig. 43).

materials, "Q" and "S", the use of the procedure as recommended by ISO 16808:2014 leads, respectively, to similar and higher absolute values of error than the use of Eq. (25). This equation overestimates the stress paths and, consequently, the sign of the stress error changes. In all other CB2001 cases, for which Eq. (25) underestimates the stress path (see Fig. 43), the proposed methodology minimizes the errors, especially when the strain path is further away from the equibiaxial.

In summary, the measurement of the strain path during the bulge test, which can be performed by means of an optical device, allows to estimate the stress path by using Eq. (25), which combined with Eq. (9) gives the principal stresses and, consequently, the von Mises equivalent stress. Finally, Eq. (26) allows the estimate of the equivalent strain. This leads to a more accurate determination of the biaxial stress *vs.* plastic strain curve, mainly for materials with strong anisotropy.

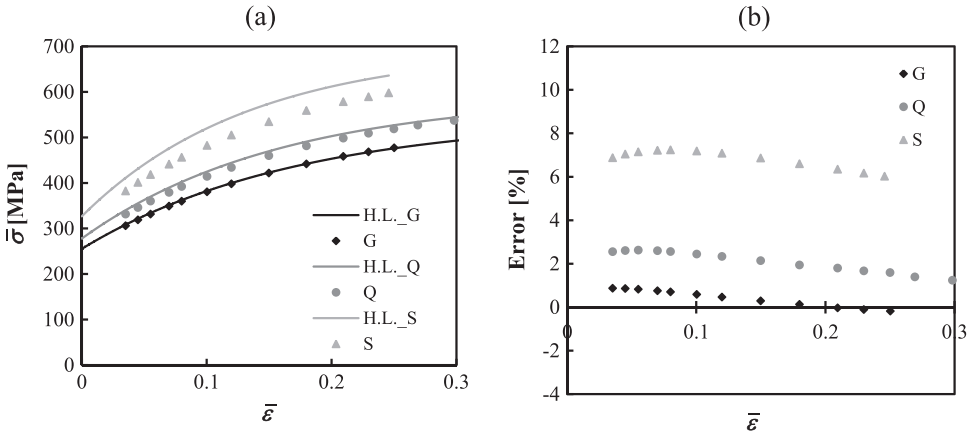

Fig. 48. (a) Comparison between the hardening laws of CB2001 materials "G", "Q" and "S" in Table 6 (lines) and the results obtained by the membrane theory (symbols) with $\sigma_1=\sigma_2=\sigma=\bar{\sigma}$ (Eq. (18)). The equivalent strain determination uses the measured values of ε_1 and ε_2 in Eq. (23); (b) evolution of the error in equivalent stress with the equivalent strain (see Fig. 43).

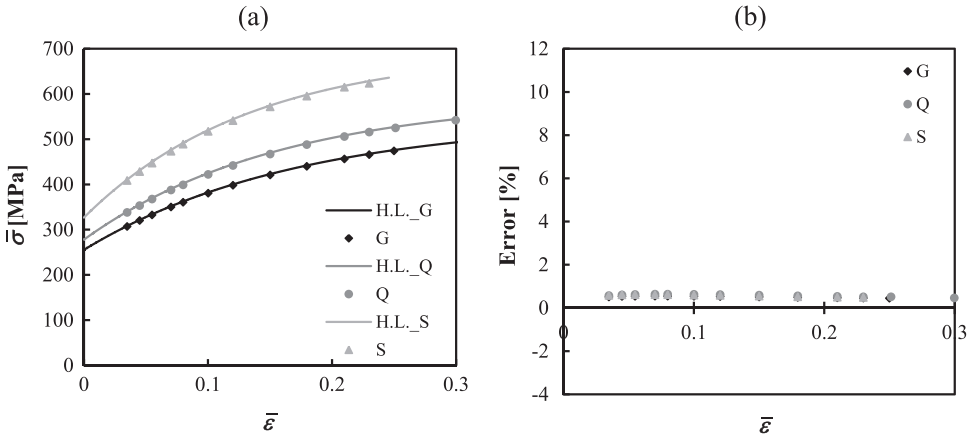

Fig. 49. (a) Comparison between the hardening laws of CB2001 materials "G", "Q" and "S" in Table 6 (lines) and the results obtained with membrane theory (symbols) using the CB2001 equivalent stress definition and Eq. (26); (b) evolution of the error in equivalent stress with the equivalent strain.

6. Conclusions

An extensive numerical study involving materials with various isotropic and anisotropic behaviours in the sheet plane, described by the Hill'48 criterion, and hardening behaviour described by the Swift law, with three hardening coefficients, $n=0.10$, 0.20 and 0.35, was performed in order to determine the biaxial stress *vs.* strain and respective errors in stress, when using the standard procedures for analysing the bulge test results.

The analysis of the geometry of the cap shows that, at each moment of the test, the geometry is quite similar for both orthotropic directions in the sheet plane, whatever the material anisotropy. This allows simplifying the use of the membrane theory ($\rho_1=\rho_2$, in Eq. (1)), since the radius of curvature is equal for both principal axes, O_1 and O_2, parallel to the orthotropic axes, O*x* and O*y*. Also, the sheet thickness as well as the equivalent stress and strain are equal, along both orthotropic axes, up to a relatively large distance from the centre of the cap.

Equibiaxial stress and strain paths are observed at the pole of the cap in the case of in-plane isotropic materials, as would be expected, but this is not the case of anisotropic materials when the ratio between both measured principal strains in the sheet plane is different from 1. In this latter case, the inability of occurrence of equibiaxial stress and strain paths is a natural consequence of the normality condition between the stress and the increment of strain (see Fig. 14).

The errors associated with the approach traditionally used, which considers equibiaxial stress (and eventually strain) paths at the pole of the cap, isotropy and the simplified equation of the membrane theory, were quantified according to the anisotropy of the sheet. Moreover, an empirical equation for the circular bulge test relating the stress path with the strain path at the pole of the cap ($\sigma_2/\sigma_1=(\varepsilon_2/\varepsilon_1)^{-2}$) is suggested to be used, regardless of the yield criterion that better describes the anisotropic behaviour of the material. This equation is based on Hill'48 results, but it was tested for two non-quadratic yield criteria, the Drucker+L and CB2001. It allows determining the stress path based on the knowledge of the strain path, which can be assessed by digital image correlation. In this context, the use of the simplified equation of the membrane theory (Eq. (10)) can be overcome by using the general equation of the membrane theory (Eq. (9)) combined with Eq. (25). It is also suggested a procedure to determine the equivalent strain (Eq. (26)), based on the plastic work definition, to be used under the condition that both stress and strain paths are known. This greatly improves the accuracy of the stress *vs.* strain curve, mainly in case of materials with strong anisotropy.

Acknowledgements

The authors gratefully acknowledge the financial support of the Portuguese Foundation for Science and Technology (FCT), Portugal, *via* Projects PTDC/EMS-TEC/0702/2014 (POCI-01-0145-FEDER-016779), PTDC/EMS-TEC/6400/2014 (POCI-01-0145-FEDER-016876), and UID/EMS/00285/2013, by UE/FEDER through Program COMPETE2020. P.A. Prates, was supported by a grant for scientific research from the Portuguese Foundation for Science and Technology (ref. SFRH/BPD/101465/2014). All supports are gratefully acknowledged.

References

[1] Chaparro BM, Thuillier S, Menezes LF, Manach PY, Fernandes JV. Material parameters identification: gradient-based, genetic and hybrid optimization algorithms. Comput Mater Sci 2008;44:339–46. http://dx.doi.org/10.1016/j.commatsci.2008.03.028.

[2] Flores P, Duchene L, Bouffioux C, Lelotte T, Henrard C, Pernin N, et al. Model identification and FE simulations: effect of different yield loci and hardening laws in sheet forming. Int J Plast 2007;23:420–49. http://dx.doi.org/10.1016/j.ijplas.2006.05.006.

[3] Rabahallah M, Balan T, Bouvier S, Bacroix B, Barlat F, Chung K, et al. Parameter identification of advanced plastic strain rate potentials and impact on plastic anisotropy prediction. Int J Plast 2009;25:491–512. http://dx.doi.org/10.1016/j.ijplas.2008.03.006.

[4] Pereira AFG, Prates PA, Sakharova NA, Oliveira MC, Fernandes JV. On the identification of kinematic hardening with reverse shear test. Eng Comput 2015;31:681–90. http://dx.doi.org/10.1007/s00366-014-0369-7.

[5] Prates PA, Oliveira MC, Fernandes JV. Identification of material parameters for thin sheets from single biaxial tensile test using a sequential inverse identification strategy. Int J Mater Form 2016;9:547–71. http://dx.doi.org/10.1007/s12289-015-1241-z.

[6] Prates PA, Oliveira MC, Fernandes JV. A new strategy for the simultaneous identification of constitutive laws parameters of metal sheets using a single test. Comput Mater Sci 2014;85:102–20. http://dx.doi.org/10.1016/j.commatsci.2013.12.043.

[7] Reis LC, Prates PA, Oliveira MC, Santos AD, Fernandes JV. Inverse identification of the Swift law parameters using the bulge test, Int J Mater Form, http://dx.doi.org/10.1007/s12289-016-1296-5.

[8] Prates PA, Pereira AFG, Sakharova NA, Oliveira MC, Fernandes JV. Inverse strategies for identifying the parameters of constitutive laws of metal sheets. Adv Mater Sci Eng 2016. http://dx.doi.org/10.1155/2016/4152963. Article ID 4152963.

[9] Koç M, Billur E, Cora ÖN. An experimental study on the comparative assessment of hydraulic bulge test analysis methods. Mater Des 2011;32:272–81. http://dx.doi.org/10.1016/j.matdes.2010.05.057.

[10] Santos AD, Teixeira P, Barlat F. Flow stress determination using hydraulic bulge test and a mechanical measurement system. In: Proceedings of the international deep drawing research group conference, IDDRG. Bilbao, Spain: IDDRG; 2011. p. 91–100.

[11] Chen K, Scales M, Kyriakides S, Corona E. Effects of anisotropy on material hardening and burst in the bulge test. Int J Solids Struct 2016;82:70–84. http://dx.doi.org/10.1016/j.ijsolstr.2015.12.012.

[12] Reis LC, Rodrigues CA, Oliveira MC, Sakharova NA, Fernandes JV. Characterization of the plastic behaviour of sheet metal using the hydraulic bulge test. In: Andrade-Campos A, Lopes N, Valente RAF, Varum H, editors. Proceedings of the first ECCOMAS young investigators conference computational methods in applied sciences. Aveiro, Portugal; 2012. p. 67.

[13] Alves JL, Bouvier S, Oliveira MC, Menezes LF. Drawbeads: to be or not to be. AIP Conf Proc, vol. 778. AIP; 2005. p. 655–60. ⟨https://dx.doi.org/10.1063/1.2011297⟩.

[14] Hsu TC, Shang HM. Mechanics of sheet metal formed by hydraulic pressure into axisymmetrical shells. Exp Mech 1976;16:337–42. http://dx.doi.org/10.1007/BF02330250.

[15] Hill R. A theory of the plastic bulging of a metal diaphragm by lateral pressure. Lond Edinb Dublin Philos Mag J Sci 1950;41:1133–42. http://dx.doi.org/10.1080/14786445008561154.

[16] Young RF, Bird JE, Duncan JL. An automated hydraulic bulge tester. J Appl Metalwork 1981;2:11–8. http://dx.doi.org/10.1007/BF02833994.

[17] Martins B, Teixeira P, Santos AD. Study on the flow stress determination using hydraulic bulge test. In: Andrade-Campos A, Lopes N, Valente RAF, Varum H, editors. Proceedings of the first ECCOMAS young investigators conference computational methods in applied sciences. Aveiro, Portugal; 2012.

[18] Bleck W, Blumbach M. Laser-aided flow curve determination in hydraulic bulging. Steel Res Int 2005;76:125–30.

[19] Mulder J, Vegter H, Aretz H, van den Boogaard AH. Accurate evaluation method for the hydraulic bulge test. Key Eng Mater 2013;554–557:33–40. http://dx.doi.org/10.4028/www.scientific.net/KEM.554-557.33.

[20] Lăzărescu L, Comşa D-S, Banabic D. Analytical and experimental evaluation of the stress-strain curves of sheet metals by hydraulic bulge tests. Key Eng Mater 2011;473:352–9. http://dx.doi.org/10.4028/www.scientific.net/KEM.473.352.

[21] DIN EN ISO 16808:2014-11 (E). Metallic materials – sheet and strip – determination of biaxial stress-strain curve by means of bulge test with optical measuring systems. BSI; 2014.

[22] Mulder J, Vegter H, Aretz H, Keller S, van den Boogaard AH. Accurate determination of flow curves using the bulge test with optical measuring systems. J Mater Process Technol 2015;226:169–87. http://dx.doi.org/10.1016/j.jmatprotec.2015.06.034.

[23] Lemoine X, Sriram S, Kergen R. Flow curve determination at large plastic strain levels to accurately constitutive equations of AHSS in forming simulation. AIP Conf Proc 2011;1353:1411–6. http://dx.doi.org/10.1063/1.3589715.

[24] Yoshida K. Evaluation of stress and strain measurement accuracy in hydraulic bulge test with the aid of finite-element analysis. ISIJ Int 2013;53:86–95. http://dx.doi.org/10.2355/isijinternational.53.86.

[25] Menezes LF, Teodosiu C. Three-dimensional numerical simulation of the deep-drawing process using solid finite elements. J Mater Process Technol 2000;97:100–6. http://dx.doi.org/10.1016/S0924-0136(99)00345-3.

[26] Oliveira MC, Alves JL, Menezes LF. Algorithms and strategies for treatment of large deformation frictional contact in the numerical simulation of deep drawing process. Arch Comput Methods Eng 2008;15:113–62. http://dx.doi.org/10.1007/s11831-008-9018-x.

[27] Neto DM, Oliveira MC, Menezes LF. Surface smoothing procedures in computational contact mechanics. Arch Comput Methods Eng 2015:1–51. http://dx.doi.org/10.1007/s11831-015-9159-7.

[28] Hill R. A theory of the yielding and plastic flow of anisotropic metals. Proc R Soc A Math Phys Eng Sci 1948;193:281–97. http://dx.doi.org/10.1098/rspa.1948.0045.

[29] Swift HW. Plastic instability under plane stress. J Mech Phys Solids 1952;1:1–18. http://dx.doi.org/10.1016/0022-5096(52)90002-1.

[30] Santos AD, Teixeira P, Barata da Rocha A, Barlat F, Moon YH, Lee M-G. On the determination of flow stress using bulge test and mechanical measurement. In: Barlat F, Moon YH, Lee MG, editors. Proceedings of the 10th international conference on NUMIFORM. Pohang, Republic of Korea: American Institute of Physics; 2010. p. 845–52. ⟨https://dx.doi.org/10.1063/1.3457644⟩.

[31] Alves JL. Simulação numérica do processo de estampagem de chapas metálicas: modelação mecânica e métodos numéricos (Ph.D. thesis). Portugal: Universidade do Minho; 2003.

[32] Reis LC, Oliveira MC, Santos AD, Fernandes JV. On the determination of the work hardening curve using the bulge test. Int J Mech Sci 2016;105:158–81. http://dx.doi.org/10.1016/j.ijmecsci.2015.11.009.

[33] Reis LC, Prates PA, Oliveira MC, Sakharova NA, Fernandes JV. Caracterização do comportamento plástico de chapas metálicas com recurso ao ensaio de expansão biaxial simétrica. In: Tadeu A, Figueiredo IN, Menezes LF, Mendes PA, Rodríguez-Ferran A, Arias I, editors. Congresso de Métodos Numéricos em Engenharia. Coimbra, Portugal: APMTAC; 2011. p. 54.

[34] Banabic D. Sheet metal forming processes – constitutive modelling and numerical simulation. Germany: Springer Berlin Heidelberg; 2010. http://dx.doi.org/10.1007/978-3-540-88113-1.

[35] Cazacu O, Barlat F. Generalization of drucker's yield criterion to orthotropy. Math Mech Solids 2001;6:613–30. http://dx.doi.org/10.1177/108128650100600603.

[36] Drucker DC. Relation of experiments to mathematical theories of plasticity. J Appl Mech ASME 1949;16:349–57.

[37] Barlat F, Aretz H, Yoon JW, Karabin ME, Brem JC, Dick RE. Linear transformation-based anisotropic yield functions. Int J Plast 2005;21:1009–39. http://dx.doi.org/10.1016/j.ijplas.2004.06.004.

[38] Voce E. The relationship between stress and strain for homogeneous deformations. J Inst Met 1948;74:537–62.

[39] Dowling NE. Mechanical behavior of materials: engineering methods for deformation, fracture, and fatigue. 2nd ed. Upper Saddle River, NJ: Prentice Hall; 1999.

[40] Lemoine X, Iancu A, Ferron G. Flow curve determination at large plastic strain levels: limitations of the membrane theory in the analysis of the hydraulic bulge test. In: Proceedings of the 14th international ESAFORM conference on material forming; 2011. p. 1411–6. ⟨https://dx.doi.org/10.1063/1.3589714⟩.

[41] Ranta-Eskola AJ. Use of the hydraulic bulge test in biaxial tensile testing. Int J Mech Sci 1979;21:457–65. http://dx.doi.org/10.1016/0020-7403(79)90008-0.

[42] M & M Research Inc. NXT defect evaluator; 2007.

[43] Prates PA, Oliveira MC, Fernandes JV. On the equivalence between sets of parameters of the yield criterion and the isotropic and kinematic hardening laws. Int J Mater Form 2015;8:505–15. http://dx.doi.org/10.1007/s12289-014-1173-z.